Defence Research and Development Canada
Recherche et développement pour la défense Canada

DEFENCE R&D DÉFENSE

A Simulation Study of Multi-Channel RADARSAT-2 GMTI

S. Chiu

Defence R&D Canada – Ottawa
TECHNICAL MEMORANDUM
DRDC Ottawa TM 2006-209
November 2006

Canada

A Simulation Study of Multi-Channel RADARSAT-2 GMTI

S. Chiu
Defence R&D Canada – Ottawa

Defence R&D Canada – Ottawa
Technical Memorandum
DRDC Ottawa TM 2006-209
November 2006

Principal Author

Original signed by S. Chiu

S. Chiu

Approved by

Original signed by Doreen Dyck

Doreen Dyck
Head/Radar Systems Section

Approved for release by

Original signed by Cam Boulet

Cam Boulet
Head/Document Review Panel

Abstract

Accurate ground moving target indication (GMTI) and target parameter estimation can be achieved only after sufficient suppression of interfering stationary clutter, particularly for space-based SARs with typically small exo-clutter regions. In its simplest form, this is accomplished using two radar receiver channels, such as the dual receive antenna mode of RADARSAT-2's Moving Object Detection EXperiment (MODEX). In this mode of operation, the full antenna is broken up into two sub-apertures with two parallel receivers to create two independent phase centres. It is well known, however, that a two-aperture approach to GMTI is sub-optimum and that target parameter estimation is often compromised by clutter interference or poor signal-to-clutter ratios. Two degrees-of-freedom are simply not enough to simultaneously suppress the clutter and to accurately estimate the target's properties, such as velocity and location.

The investigation, described in this Technical Memorandum, explores several concepts of increasing the spatial diversity for RADARSAT-2, which allows the two-channel SAR system to operate like a three or four channel radar. Owing to the very flexible programming capabilities of the RADARSAT-2 antenna, this can either be accomplished by the toggling of the transmitter between subsequent pulses or via clever transmitter/receiver excitation schemes. A trade-off analysis between number of channels, phase centre separations, and PRF limitations is presented for a system based on RADARSAT-2 MODEX parameters.

Résumé

La précision des indications de cible terrestre mobile (GMTI) et des estimations de paramètres des cibles dépend uniquement d'une suppression suffisante du clutter fixe, surtout pour les ROS spatiaux à régions d'exoclutter typiquement réduites. Sous sa forme la plus simple, ce résultat s'obtient au moyen de deux canaux de récepteur radar, par exemple dans le mode à antenne de réception double utilisé pour l'expérience de détection des objets mobiles (MODEX) de RADARSAT-2. Dans ce mode de fonctionnement, l'antenne complète est subdivisée en deux sous-ouvertures associées à deux récepteurs parallèles créant deux centres de phase indépendants. On sait bien, toutefois, que la technique des deux ouvertures n'est pas optimale pour les applications GMTI et que l'estimation des paramètres des cibles est souvent compromise par le brouillage dû au clutter ou par de mauvais rapports signal/clutter. Deux degrés de liberté ne suffisent tout simplement pas pour, simultanément, supprimer le clutter et estimer avec précision les propriétés des cibles, comme la vitesse et la position. L'étude décrite dans le présent document technique examine plusieurs aspects de l'accroissement de la diversité spatiale de RADARSAT-2, qui permet de faire fonc-

tionner le système SAR à deux canaux comme un radar à trois ou à quatre canaux. En raison de la très grande souplesse de programmation de l'antenne RADARSAT-2, ce résultat peut s'obtenir soit par le basculement de l'émetteur entre des impulsions subséquentes, soit par d'ingénieux systèmes d'excitation d'émetteur et de récepteur. Une analyse de compromis entre le nombre de canaux, l'espacement des centres de phase et les limites de fréquence de répétition des impulsions (FRI) est présentée pour un système basé sur les paramètres MODEX de RADARSAT-2.

Executive summary

A Simulation Study of Multi-Channel RADARSAT-2 GMTI

S. Chiu; DRDC Ottawa TM 2006-209; Defence R&D Canada – Ottawa; November 2006.

Background: Canada's RADARSAT-2 spaceborne SAR will be launched in 2007. This SAR can be operated in an experimental ground moving target indication (GMTI) mode called MODEX for Moving Object Detection EXperiment. In this mode of operation, the radar antenna is split into two sub-apertures, each with its own receiving channel, which provide scene-motion sensitivity and thus permit moving targets to be detected and their velocity parameters estimated. However, a severe GMTI limitation exists for the two-aperture radar system due to contamination of moving target signals by clutter. This limitation has motivated the exploration of multi-channel concepts using aperture toggling or switching techniques, which allow a radar with two physical apertures to behave like a multi-aperture system by generating virtual phase centres. Three multi-channel conceptual modes for the RADARSAT-2 type imaging radar are proposed, examined and tested in this Technical Memorandum.

Principal results:

Multi-channel concepts

Three multi-phase centre modes for the RADARSAT-2 MODEX are proposed. The first is a three-channel toggle-transmit mode, in which the radar alternately transmits using the fore and aft sub-apertures and receives echoes with both sub-apertures simultaneously. The second and third multi-channel schemes are three-channel and four-channel toggle-receive modes, respectively. In these modes, the radar transmits using the full aperture but receives echoes with different sub-sections of the aperture on alternating pulses. The three-channel toggle-transmit mode has the same along-track baseline as the original two-aperture system. However, for both of the three-channel and four-channel toggle-receive modes the baseline is half of that for the two-aperture system. A shorter along-track baseline will usually lead to lower sensitivity to slowly moving targets. On the other hand, a higher degree of freedom (i.e. the number of available channels) may improve the detection performance, which may compensate for this reduced baseline.

Beamwidth and sidelobe level trade-offs

Different combinations of transmit/receive aperture sizes yield different two-way antenna patterns with the accompanying variations in sidelobe levels and beamwidths. The widest beamwidth (but not the highest sidelobe levels) is generated using half antenna transmit and half antenna receive (i.e. the toggle-transmit mode). The antenna pattern generated for the full-antenna transmit and quarter antenna receive (i.e. the four-channel toggle-receive mode) does not differ significantly from the full-antenna transmit and half-antenna receive case (or the two-aperture receive mode).

Improvement in ATI phase estimation and moving target detection

Multi-channel GMTI performance using the simple DPCA detection metric is found to improve as a function of the number of available channels for a constant separation of phase centres. Similarly, the estimation of the along-track interferometric phase, which is proportional to the radial velocity of a moving target, is shown to improve in accuracy with an increasing number of channels. These results apply only to the constant baseline case. Increasing the number of channels at the expense of reducing the baseline may not lead to an overall improvement in GMTI performance.

Multi-channel clutter cancellation

The key question concerning the generation of three or four phase centres from a two-channel SAR system is, "Can these virtual phase centres generated using aperture toggling be effectively used to suppress the stationary background clutter?" Simulation experiments which mimic the three proposed multi-channel modes clearly show that the stationary clutter can be effectively cancelled using phase centres generated via sub-aperture toggling in such a way that the interferometric phase of a moving target can be more accurately estimated.

Significance of results: The feasibility of applying the aperture toggling or switching concept to the RADARSAT-2 multi-channel MODEX is demonstrated here for the first time using simulation. Although the application of this concept to multi-channel GMTI is not new, the "proof" of the concept is presented here. This conclusive result leads to the real possibility of RADARSAT-2 multi-channel MODEX modes: these were not considered possible in the initial designs of the MODEX.

Future work: Future work should include full-scale simulation experiments using SBRMTISIM (the Space-Based Radar Moving Target Indication Simulator) to investigate the advantages and disadvantages of each of the proposed modes.

Sommaire

A Simulation Study of Multi-Channel RADARSAT-2 GMTI

S. Chiu; DRDC Ottawa TM 2006-209; R & D pour la défense Canada – Ottawa; novembre 2006.

Contexte: Le SAR spatial RADARSAT-2 du Canada sera lancé en 2007. Ce SAR peut fonctionner dans un mode expérimental d'indication de cible terrestre mobile (GMTI) appelé MODEX, pour " Moving Object Detection EXperiment " (expérience de détection des objets mobiles). Dans ce mode de fonctionnement, l'antenne radar est subdivisée en deux sous-ouvertures, dotées chacune de leur propre canal de réception, qui procurent une sensibilité au mouvement des scènes et permettent ainsi de détecter les cibles mobiles et d'estimer leurs paramètres de vitesse. Le système radar à deux ouvertures présente toutefois une grave limitation en matière de GMTI, en raison de la contamination des signaux de cibles mobiles par le clutter. Cette limitation a stimulé la recherche sur les systèmes multicanaux utilisant des techniques de basculement ou de commutation d'ouvertures, grâce auxquelles le radar à deux ouvertures matérielles se comporte comme un système à ouvertures multiples en créant des centres de phase virtuels. Le présent document technique propose, examine et évalue trois conceptions de modes multicanaux pour le radar d'imagerie de type RADARSAT-2.

Résultats:

Techniques multicanaux

Trois modes à centres de phase multiples sont proposés pour MODEX de RADARSAT-2. Le premier est un mode d'émission par basculement à trois canaux, dans lequel le radar émet en alternance dans les sous-ouvertures avant et arrière et reoit les échos en utilisant simultanément les deux sous-ouvertures. Les deuxième et troisième modes font respectivement appel à des techniques de réception par basculement à trois canaux et à quatre canaux. Dans ces modes, le radar émet dans l'ouverture complète, mais reoit les échos dans des sous-sections différentes de l'ouverture, au moyen d'impulsions en alternance. Le mode d'émission par basculement à trois canaux offre la même ligne de base longitudinale que le système original à deux ouvertures. Toutefois, pour les modes de réception par basculement à trois canaux et à quatre canaux, la ligne de base correspond à la moitié de celle du système à deux ouvertures. Une ligne de base longitudinale plus courte donne habituellement une sensibilité plus basse aux cibles mobiles lentes. Par ailleurs, un degré de liberté supérieur (nombre de canaux disponibles) peut améliorer le rendement de détection et compenser ainsi la réduction de la ligne de base.

Compromis entre la largeur du faisceau et le niveau des lobes latéraux

Différentes combinaisons de taille des ouvertures d'émission et de réception produisent différents diagrammes d'antenne bidirectionnels et des variations correspondantes touchant le niveau des lobes latéraux et la largeur du faisceau. La plus grande largeur de faisceau (mais pas le niveau le plus élevé des lobes latéraux) s'obtient pour une émission sur demi-antenne et une réception sur demi-antenne (c.-à-d. dans le mode d'émission par basculement). Le diagramme d'antenne produit pour une émission sur antenne complète et une réception sur quart d'antenne (c.-à-d. dans le mode de réception par basculement à quatre canaux) ne diffère pas beaucoup de l'émission sur antenne complète et de la réception sur demi-antenne (c.-à-d. le mode de réception à deux ouvertures).

Amélioration de l'estimation de la phase interférométrique longitudinale et de la détection des cibles mobiles

Il est démontré que le rendement de GMTI multicanaux fondé sur de simples mesures de détection avec antennes à centre de phase déplacé (DPCA) s'améliore en fonction du nombre de canaux disponibles pour un espacement constant des centres de phase. De même, il s'avère que l'estimation de la phase interférométrique longitudinale, qui est proportionnelle à la vitesse radiale d'une cible mobile, augmente de précision lorsque le nombre de canaux s'accroît. Ces résultats s'appliquent seulement au cas de la ligne de base constante. L'augmentation du nombre de canaux, au détriment d'une réduction de la ligne de base, peut ne pas entraîner d'augmentation globale du rendement de GMTI.

Annulation de clutter multicanaux

La production de trois ou quatre centres de phase dans un système ROS à deux canaux soulève une question essentielle : ces centres de phase virtuels produits par basculement d'ouverture peuvent-ils s'utiliser efficacement pour supprimer le clutter de fond fixe ? Des expériences de simulation imitant les trois modes multicanaux proposés démontrent clairement la possibilité d'une annulation efficace du clutter fixe au moyen des centres de phase produits par le basculement de sous-ouverture, de faon que la phase interférométrique d'une cible mobile puisse s'estimer avec plus de précision.

Portée: La possibilité d'utiliser la technique de basculement ou de commutation d'ouverture pour l'application MODEX multicanaux de RADARSAT-2 est démontrée ici pour la première fois au moyen d'une simulation. Bien que l'application de cette

technique à la GMTI multicanaux ne soit pas nouvelle, la " preuve " de conception en est présentée ici. Ce résultat concluant soulève la réelle possibilité de modes MODEX multicanaux pour RADARSAT-2, ce qui n'était pas considéré comme possible durant les étapes initiales de conception de MODEX.

Recherches futures: Les recherches futures devraient comprendre des expériences de simulation complète au moyen de SBRMTISIM (simulateur d'indication de cibles mobiles de radar spatial) en vue d'examiner les avantages et les inconvénients de chacun des modes proposés.

This page intentionally left blank.

Table of contents

List of figures

This page intentionally left blank.

1 Introduction

Canada's RADARSAT-2 commercial spaceborne SAR, to be launched in 2007, can be operated in an experimental mode (called MODEX for Moving Object Detection EXperiment) which will allow the full antenna to be broken into two sub-apertures with two parallel receivers to define two independent data channels [2]. These two sub-apertures in the flight direction can be used to record two echoes (the dual-receive mode), one from each wing for every pulse transmitted using the full antenna. The two apertures make it possible to detect targets with non-zero across-track velocity by providing two identical views of the observed scene obtained at slightly different times. Recently, several new detection techniques for two-channel SAR ground moving target indication (GMTI), including their statistical performance, have been proposed, e.g. [3]. It is well known that quasi-optimum detection and parameter estimation can be achieved if at least three physical phase centres are available [4] [5] [6]: Two degrees-of-freedom are not enough to simultaneously suppress the clutter and to accurately estimate the target's properties, such as velocity and location.

Although the design of RADARSAT-2 only permits the simultaneous use of two receivers, an alternating transmit mode (or the toggle-transmit mode [10]) is anticipated to provide a third independent phase centre [11]. In this toggle-transmit mode, pulses are alternately transmitted from the fore and aft apertures and are simultaneously received using both apertures. This mode not only allows greater separation of the two-way phase centres in the along-track direction but also the possibility of generating a third phase centre for three-aperture GMTI. In addition to this mode of operation, the very flexible programming capabilities of the RADARSAT-2 antenna allow the two-channel SAR system to operate practically like a three or four channel radar using schemes of well-designed transmitter/receiver excitation.

This Technical Memorandum begins by describing concepts of RADARSAT-2 multi-channel modes, followed by analysis and demonstration of the performance gains for SAR-GMTI by the exploitation of additional channels. The results of simulation experiments are presented.

2 Multi-Channel Concepts

Several multi-aperture concepts have been explored. These are illustrated in Fig. 1. By doubling the pulse repetition frequency (PRF) of the radar, it is possible to generate third and fourth phase centres using the three basic schemes as illustrated. The first one, Fig. 1(a), uses the so-called toggle-transmit mode, in which the radar alternately transmits using its fore and aft sub-apertures and receives the echoes with both sub-apertures simultaneously. This scheme allows the generation of three phase

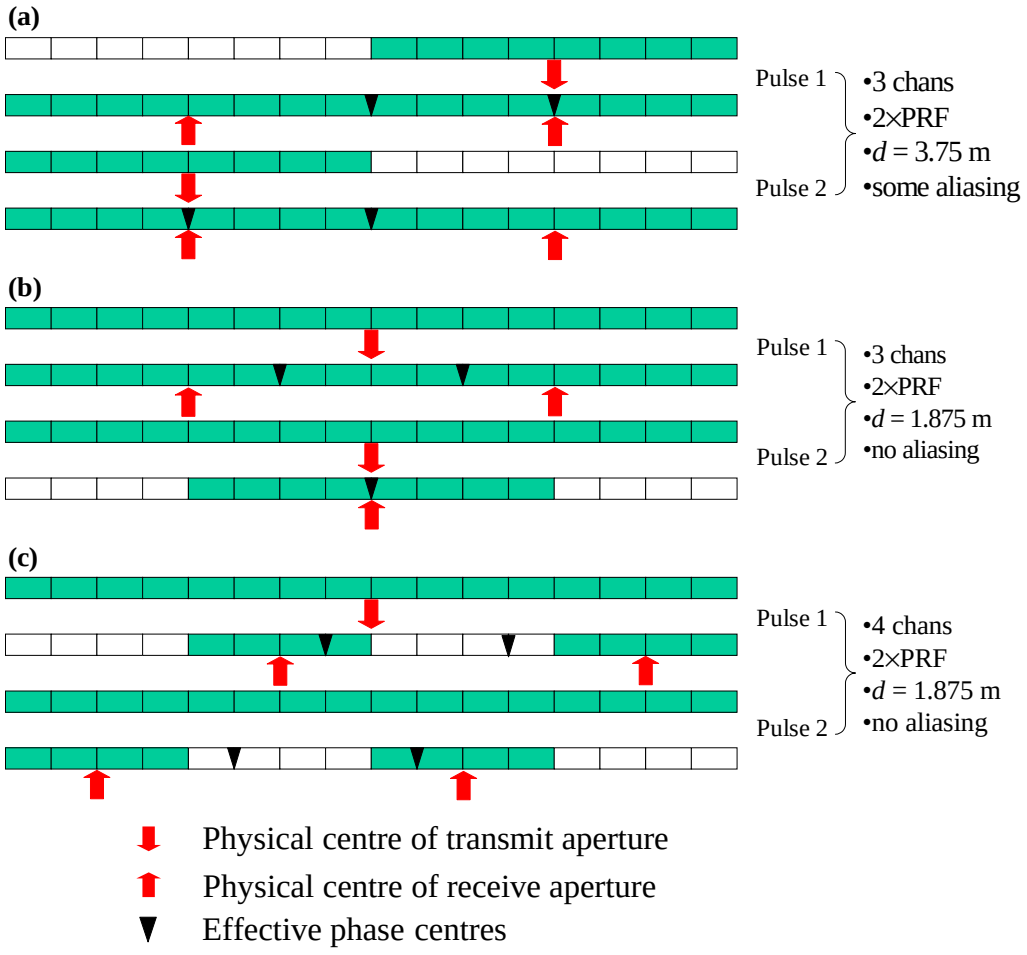

Figure 1: *Concepts of increasing the spatial diversity for RADARSAT-2, allowing the two-channel SAR system to effectively operate as a three or four channel radar. This can either be accomplished by transmitter toggling between subsequent pulses or via receiver excitation and toggling schemes.*

centres as indicated by the black triangles in Fig. 1. The two "side" phase centres are used to sample radar echoes at half the rate of the middle phase centre. Therefore, in order to avoid the aliasing of the"clutter band," it is necessary to double the pulse repetition frequency (PRF) of the radar. However, the PRF is not the only parameter of concern. Since the radar is now transmitting at half the antenna width, there is a broadening of the physical beamwidth, which increases the clutter bandwidth and, in turn, the aliasing of the clutter band. This beam broadening will be the subject of the next section. For now, it is noted that there may be a small aliasing with this mode of operation given that the Doppler spectrum as given by the 3-dB beamwidth is about 3752 Hz whereas the maximum RADARSAT-2 PRF is only 3800 Hz. The along-track baseline of this approach is twice as large as that for the other two schemes. The longer baseline will permit the detection of slower moving targets, because the along-track interferometric phase of a moving target is proportional to the baseline.

The second and the third schemes, instead of using different sub-apertures on transmit, use different sub-apertures on receive. This is accomplished by "turning off" different regions of the antenna on receive, so that echoes are sampled by different sub-panels of the antenna in an alternating manner, as illustrated in Figs. 1(b)&(c). The second scheme generates three phase centres: The middle phase centre is generated by summing the two half portions of the fore and aft sub-apertures of RADARSAT-2. The along-track baseline (the distance between phase centres) of this approach is half of that in the two-aperture along-track interferometry (ATI) but offers greater spatial diversity than the two-aperture system. It provides the advantage of an extra degree of freedom for clutter cancellation resulting in a potential improvement in target parameter estimation. Again, the PRF must be doubled to avoid aliasing. The third approach to multi-channel GMTI, Fig. 1(c), is very similar to the second scheme but produces four phase centres with the same along-track baseline as the second scheme. Different regions of sub-apertures are excited alternately at receive such that a pair of phase centres are generated for each alternating pulse. The PRF is doubled to minimize the aliasing of the clutter band. It should also be noted that there is a price to pay for increasing the PRF, since this reduces the width of the swath in slant range. This could impact the utility of this scheme for different applications.

3 Beamwidth and Sidelobe Level Trade-Offs

In this section the trade-offs in beamwidth and sidelobe level for the three proposed multi-aperture modes are examined. When partitioning a single aperture into smaller parts, the two-way beamwidth (or antenna pattern) changes. This can be easily seen in Fig. 2. The beam patterns are computed using the MATLAB code "beamForming2.m" (given in Appendix C). The different combinations of transmit/receive aperture sizes yield different two-way antenna patterns, including increased sidelobe

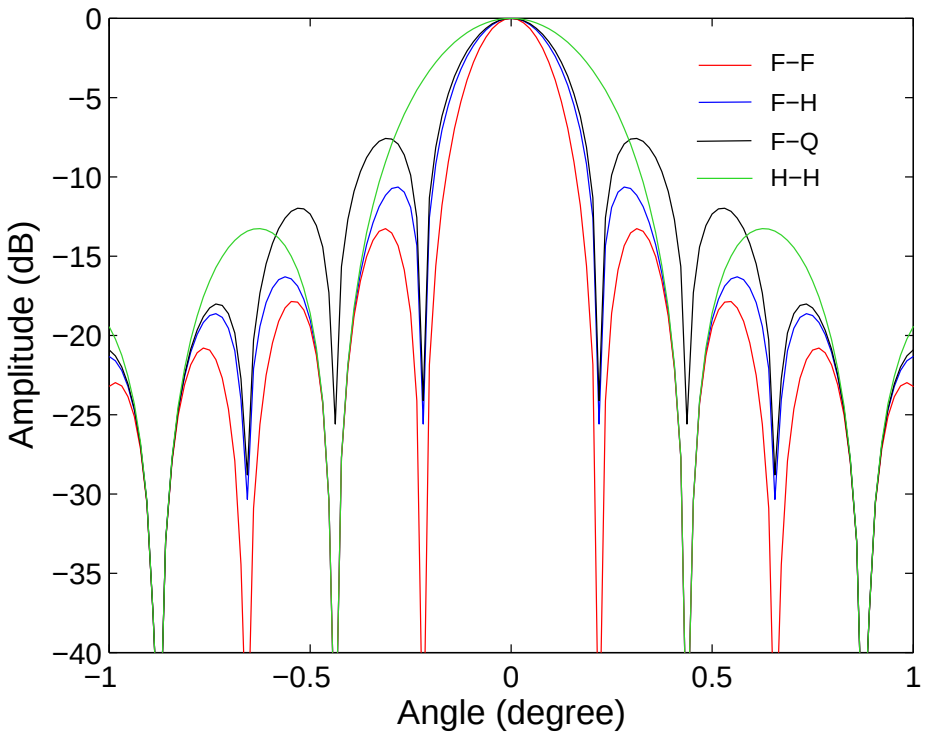

Figure 2: *The antenna patterns of different transmit and receive sub-aperture combinations showing the different resulting beamwidths and sidelobe levels. "F-F": full aperture transmit and full aperture receive, "F-H": full aperture transmit and half aperture receive, "F-Q": full aperture transmit and quarter aperture receive, and "H-H": half aperture transmit and half aperture receive.*

levels and/or increased beamwidths. The narrowest beamwidth and lowest sidelobe levels are obtained, as expected , using the full aperture on transmit and on receive. The widest beamwidth (but not the highest sidelobe levels) is generated using half of the antenna on transmit and half of the antenna on receive. It is interesting to note that the antenna patterns generated from the "F-H" (full aperture transmit and half aperture receive) and the "F-Q" (full aperture transmit and quarter aperture receive) do not differ significantly in the main beam; only their sidelobe levels are different (about 3 dB difference). This is good news since there is not a significant loss in buying these extra degrees of freedom.

The 3-dB main-beam induced clutter Doppler spread can be computed from the radar platform velocity v_a projected onto the radar-to-clutter radial direction. Assuming zero-angle beam squint, this is given by [1]

$$\Delta f_D = 2f_D = 2\left(2\frac{v_r}{\lambda}\right) = 4\frac{v_s \sin\varphi}{\lambda}, \tag{1}$$

where v_s and v_r are the spacecraft velocity and the radial component of this velocity, respectively, 2φ is the 3-dB beamwidth angle, and λ is the wavelength.

4 Moving Target Signal Model

Simulation experiments have been carried out to validate the multi-aperture concept for the RADARSAT-2 MODEX. For simplicity, the flat-earth or airborne geometry is chosen for the simulation, since the "proof" of the concept is independent of the imaging geometry. The phase history of a moving target in a flat-earth geometry, as shown in Fig. 3, can be modelled as

$$\begin{aligned}\varphi(t) &= -2kR(t) \\ &= -2k\sqrt{[x_0 + (v_{x0} - v_a)t + a_{x0}t^2/2]^2 + [y_0 + v_{y0}t + a_{y0}t^2/2]^2 + h^2},\end{aligned} \tag{2}$$

where $R(t)$ is the range history of the moving target, $k = 2\pi/\lambda$ (λ is wavelength), and v and a are target velocity and acceleration, respectively. Subscript "0" denotes values at $t = 0$, and x and y are the along-track and across-track components, respectively. The target velocity and position at broadside time t_b are therefore

$$\begin{aligned} v_{xb} &= v_{x0} + a_{x0}t_b, \\ v_{yb} &= v_{y0} + a_{y0}t_b, \\ x_b &= v_a t_b = x_0 + v_{x0}t_b + a_{x0}t_b^2/2, \\ y_b &= y_0 + v_{y0}t_b + a_{y0}t_b^2/2. \end{aligned} \tag{3}$$

The second last equation of (3) is a result of the definition of "broadside," where the azimuth position of the radar coincides with that of the moving target.

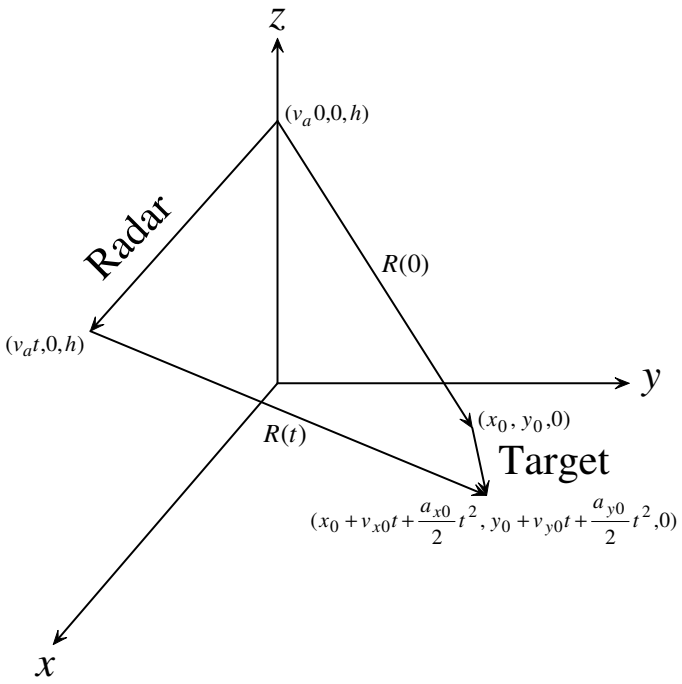

Figure 3: *A target moving with constant acceleration in a flat-earth geometry with components of motion in the x and y directions. The radar moves in the positive x direction.*

Assuming a constant-acceleration target (i.e. constant a_{x0} and a_{y0}), the Taylor series expansion of (2) about t_b can be written as

$$\begin{aligned}\varphi(t) \approx -2k\{&R_b + v_{yb}\gamma(t-t_b) \\ &+ \frac{1}{2R_b}(v_{rel}^2 + y_b a_{y0})(t-t_b)^2 \\ &+ \frac{1}{2R_b}[(v_{xb}-v_a)a_{x0} + v_{yb}a_{y0}(1-\gamma^2)](t-t_b)^3 + \ldots\},\end{aligned} \tag{4}$$

where R_b is the slant range to the target at broadside and

$$\begin{aligned}\gamma &= y_b/R_b, \\ v_{rel}^2 &= (v_{xb}-v_a)^2 + v_{yb}^2(1-\gamma^2).\end{aligned} \tag{5}$$

The detailed derivation of (4) is given in Appendix B. The "slow-time" moving target signal can, therefore, be modelled as

$$s = \text{rect}\left[\frac{t-t_b}{T}\right]e^{j\varphi(t)}, \tag{6}$$

which is a finite-time linear chirp with duration T centred at time $t = t_b$. For actual signals, the "rect" function would be modulated by the antenna pattern.

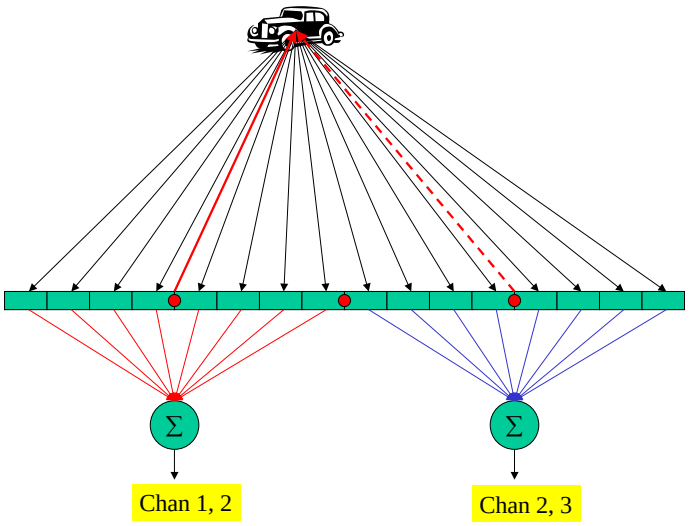

Figure 4: *Schematic showing the simulation of a multi-aperture antenna: the radar pulse is transmitted at alternating fore and aft sub-apertures (eight sub-panels each) and returns are received using 16 sub-panels. The return signals received at the 16 sub-panels are added in such a way as to form three sub-apertures with their respective phase centres.*

5 Experiments

5.1 Simulation Design

In order to test and validate the multi-channel concepts obtained by sub-aperture toggling (or switching) for a physical two-channel radar, simulation experiments can be designed in MATLAB. These mimic what actually takes place in the sampling of radar echoes using the temporal diversity strategies described in the previous section and the subsequent GMTI signal processing.

The first simulation considers the toggle-transmit mode of the RADARSAT-2 MODEX. The simulator architecture is illustrated in Fig. 4. The three phase centres are generated by alternately transmitting radar pulses using the fore and aft apertures (as shown in solid and dash-lined arrows) and sampling the echoes using sixteen sub-panels (shown as green rectangles), as for the sixteen sub-panels on RADARSAT-2. The signals received by the sixteen sub-panels are then coherently added to form channels 1 and 2 for the odd pulses and channels 2 and 3 for the even pulses. The positions of the actual phase centres on the antenna are shown as red dots in Fig. 4. The MATLAB code simulator "airMultiChan_toggle.m" is used to validate the concept and is given in Appendix E.

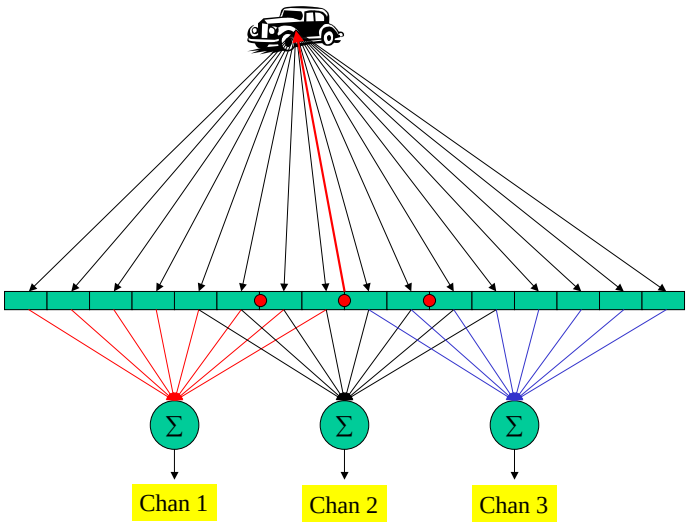

Figure 5: *Schematic showing the simulation of a multi-aperture antenna: radar signal is transmitted at full aperture and returns are received using 16 sub-panels. The return signals received at the 16 sub-panels are added in such a way as to form three sub-apertures or phase centres.*

The second multi-channel simulation architecture is illustrated in Fig. 5. The radar signal is transmitted using the full aperture and the echoes are sampled using 16 sub-panels. The signals from the 16 sub-panels are added in such a way so as to form three phase centres (shown as red dots in the figure). This architecture allows the simulation of a true multi-channel radar as well as the emulation of a multi-channel radar via temporal diversity (or switching). The three phase centres can be generated by sampling the echoes using three different sub-sections of the antenna as shown in the figure. Since RADARSAT-2 only has two channels for the sampling of return echoes, the apertures for phase centres 1 and 3 must be sampled for the odd numbered pulses and those for phase centre 2 for the even numbered pulses. The PRF must be doubled in order to maintain the original sampling rate (for each phase centre) to avoid aliasing.

The third multi-channel simulation architecture (illustrated in Fig. 6) is very similar to the previous one. In the same way, the radar pulse is transmitted at full aperture and return echoes are sampled using 16 sub-panels. Then the signals from the 16 sub-panels are added coherently to form four distinct phase centres as shown. The simulator permits the simulation of a true four-channel radar as well as the emulation of a four-channel radar via sub-aperture switching. With only two physical receiver channels of RADARSAT-2, it is necessary to sample phase centres 1 and 3 on the odd numbered pulses and phase centres 2 and 4 on the even numbered pulses. Again, the PRF must be at least doubled in order to keep the original sampling rate at each

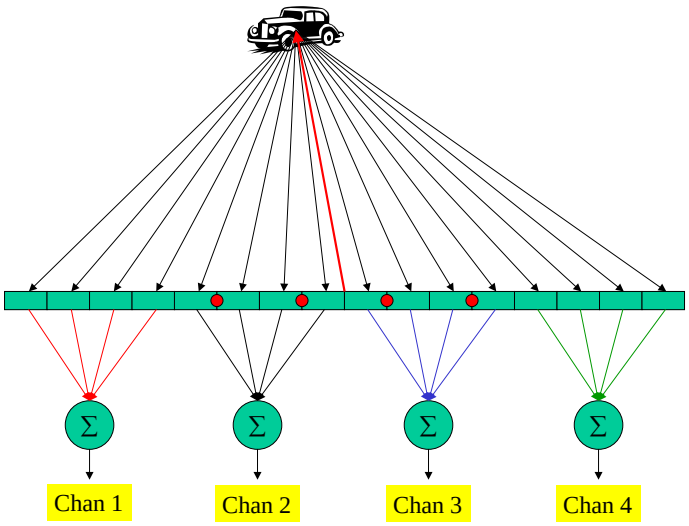

Figure 6: *Schematic showing the simulation of a multi-aperture antenna: the radar signal is transmitted using the full aperture and returns are received using 16 sub-panels. The return signals received at the 16 sub-panels are added in such a way as to form four phase centres.*

phase centre. The doubling of the PRF may not be sufficient due to the changes in the antenna patterns in the toggle modes.

5.2 Toggle-Transmit Mode

RADARSAT-2 MODEX, as mentioned earlier, is capable of emulating a third phase centre by operating in the toggle-transmit mode, thereby allowing the three-channel processing of ground moving targets. With alternating transmit and simultaneous receive using fore and aft apertures, the effective two-way 3 dB beamwidth is about 0.4° in azimuth resulting in a clutter bandwidth of 1876 kHz. As the toggle-transmit mode requires a PRF that is at least twice the clutter bandwidth, the maximum PRF for RADARSAT-2 of 3.8 kHz is only marginally above the Nyquist frequency. With the third phase centre, the interfering clutter can be cancelled before forming the interferogram by first subtracting (via DPCA) the signals in channel 2 from those in channel 1 and those in channel 3 from those in channel 2, and then forming the interferogram from the two resulting clutter-cancelled "channels." For channels 1 and 2, the phase of the DPCA output signal can be shown to be

$$\psi_{12} = \frac{2\pi(R_1 + R_2)}{\lambda} \pm \frac{\pi}{2}, \tag{7}$$

where R_1 and R_2 are the distances from the phase centres 1 and 2 to the target of interest, respectively. Similarly for channels 2 and 3, $\psi_{23} = 2\pi(R_2 + R_3)/\lambda \pm \pi/2$.

The resulting interferometric phase is thus

$$\psi = \frac{2\pi(R_1 - R_3)}{\lambda} = \frac{4\pi(R_1 - R_2)}{\lambda} = \frac{4\pi v_r \tau}{\lambda}. \quad (8)$$

The phase of the three-channel ATI, in the toggle-transmit mode, is exactly the same as that for the two-channel ATI, except the clutter has now been cancelled via the DPCA subtraction. All the parameter estimation algorithms previously derived for the two-channel ATI can now be applied in exactly the same manner without any modification. A simulation for a moving target with $v_x = -26.63$ m/s and $v_r = -10.79$ m/s in a background of Gaussian clutter (and using a matched filter perfectly matched to the target motion) shows that the target's ATI phase deviates strongly from the ideal (uncorrupted) phase value of 70.5° when the two-phase-centre ATI approach is used (see the blue curves in Fig. 7). This is believed to be due to corruption of the target signal by the overlapping stationary clutter. The ATI phase bias is a function of the signal-to-clutter ratio (SCR). With the three-phase-centre ATI, on the other hand, the clutter-cancelled target signals yield an unbiased ATI phase (as shown in the red curves of Fig. 7).

5.2.1 Can the Toggle-Transmit Mode Really Produce Three Phase Centres?

Although generating three or four phase centres from a two-channel SAR system may seem at first magical, German researchers have been using this aperture switching concept to increase spatial diversity of a two-channel radar system for many years [7] [8] [9]. The key question that needs to be answered is, "Does the toggle-transmit mode, derived from the two physical receiver channels of RADARSAT-2, really provide an independent third phase centre useable for clutter suppression?"

The simulator "airMultiChan_toggle.m" is used to generate the moving target signal ($v_x = 3$ and $v_y = -4$) embedded in a competing clutter signal. It then samples radar echoes using the strategies (to be used in the actual RADARSAT-2 signal processor), which are described earlier and generates three signal channels sampled at twice the original PRF. The clutter signals are cancelled using the procedure described above, followed by the formation of the interferogram from the "clutter-free" signals. The results of the simulator output are shown in Figs. 8(a) to 9(e).

Fig. 8(a) depicts the antenna "pattern" obtained by summing the signals received by eight sub-panels of the sixteen-panel antenna. Fig. 8(b) shows the compressed moving target signal embedded in a clutter background. The signal compression is carried out using the fractional Fourier transform [18]. Figs. 8(c) through 9(a) are time-frequency representations (via the short-time Fourier transform) of the fore aperture signals, the fore channel minus the centre channel 1, the centre channel

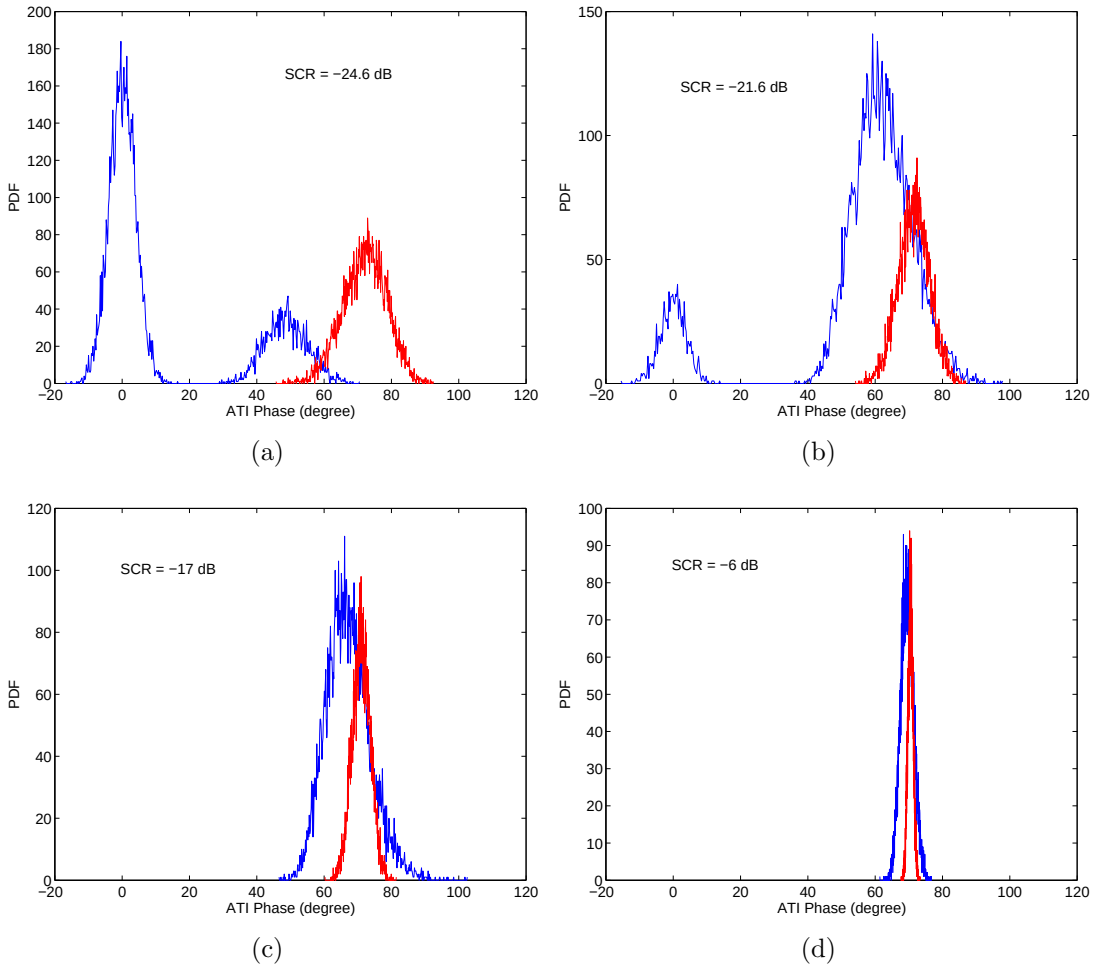

Figure 7: *A simulated deterministic target moving with $v_x = -26.63$ m/s and $v_r = -10.79$ m/s in a background Gaussian clutter. The angle of incidence is 50°, the matched filter is matched to the target motion, and the ideal ATI phase is 70.5°. The two-phase-centre and three-phase-centre results are denoted by blue and red lines, respectively. The SCR is calculated before azimuth compression; both signal and matched-filter lengths are equal to the 4 dB beam width; scene coherence $\rho = 0.95$. (a) $SCR = -24.4$ dB; (b) $SCR = -21.6$ dB; (c) $SCR = -17$ dB; (d) $SCR = -6.0$ dB.*

1 minus the aft channel, the centre channel 2 minus the aft channel, and the fore channel minus the aft channel. As can be seen, the simulation results clearly show that the generation of the third independent phase centre is indeed feasible using the toggle-transmit scheme. Figs. 8(c)-8(f) clearly demonstrate that the fore and aft channel clutter signals can be suppressed using the third (virtual) phase centre (or channel 2). The interferograms of the fore and aft channels are initially contaminated by the interfering clutter as seen in Figs. 9(b)-9(c). After the clutter cancellation, the interferogram is well defined and its phase agrees with the true phase of the moving target.

5.3 Toggle-Receive Modes

Instead of changing the antenna pattern on transmission (i.e. via excitation of different parts of the antenna), the alternative is to vary the regions of antenna excitation at reception. Radar pulses are transmitted using the full antenna aperture, and return echoes are received with sub-sections of the antenna in order to provide greater spatial diversity for more efficient clutter cancellation.

5.3.1 Improvement in ATI Phase Estimation and Detection

The key question to be answered is how these different modes of antenna excitation (with an increased number of available independent channels) affect or improve the measurement of a moving target's interferogram? In the following, simulations of the moving target's interferometric phase (contaminated by background clutter) for two, three, and four channel SAR systems are performed and ATI phase probability density functions (PDFs) as a function of the number of channels (showing improvement on accuracy of phase measurements) are shown in Fig. 10. As before, the ATI phase of the stationary clutter is centred around the zero value and the phase PDFs of a target moving at $v_x = 3$ m/s and $v_y = 4$ m/s are also shown. The conventional two-channel system, computed using only channels 1 and 2 or channels 2 and 3, yields biased ATI phase measurements (labelled as '12 & 23' on the figure). The ATI phase measured from the three-channel SAR, computed by forming an interferogram between the DPCA of channels 1 and 2 and the DPCA of channels 2 and 3 or between the DPCA of channels 2 and 3 and the DPCA of channels 3 and 4 (labelled as '123 & 234'), shows no phase biases. However, the measured phase variance can be quite large depending on the degree of clutter cancellation or the clutter coherence between the channels. When all four channels are used, the ATI phase measurements obtained by summing the interferogram measurements from channels 1 to 3 and channels 2 to 4 give an unbiased ATI phase with a noticeably smaller variance (labelled as 'ATI sum')). Also shown are the ATI phase measurements computed using the following

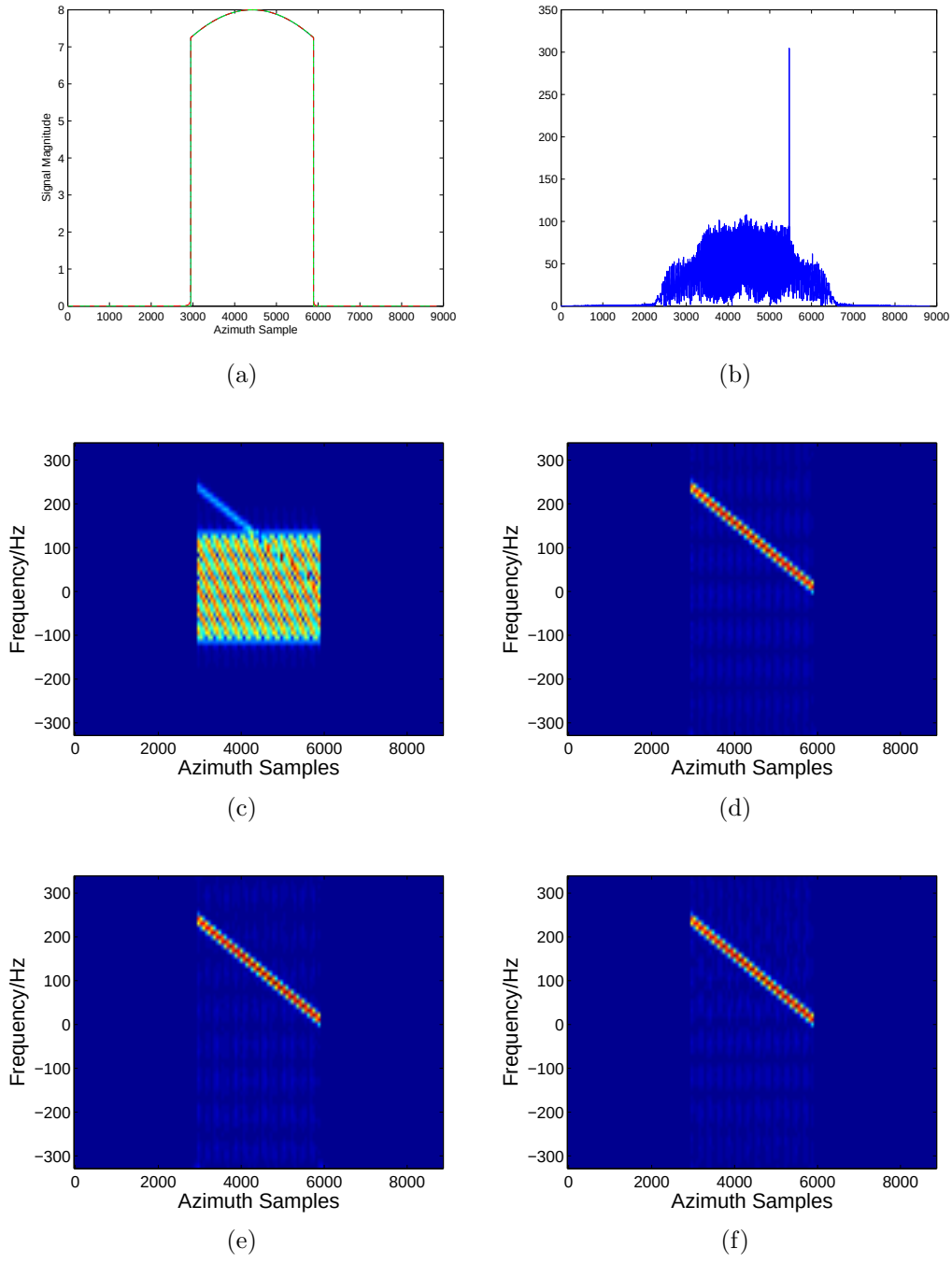

Figure 8: *Three-channel GMTI using toggle-transmit mode: alternating transmit at fore and aft half sub-apertures and receive simultaneously with two half sub-apertures. The fore and aft channels are sampled at half the rate of the centre channel. To avoid aliasing, the PRF is doubled. (a) Normalized antenna patterns, (b) fore channel signals (target plus clutter) after fractional Fourier transform compression, time-frequency plots of (c) fore aperture signals, (d) fore channel minus centre channel 1, (e) centre channel 1 minus aft channel, and (f) centre channel 2 minus aft channel.*

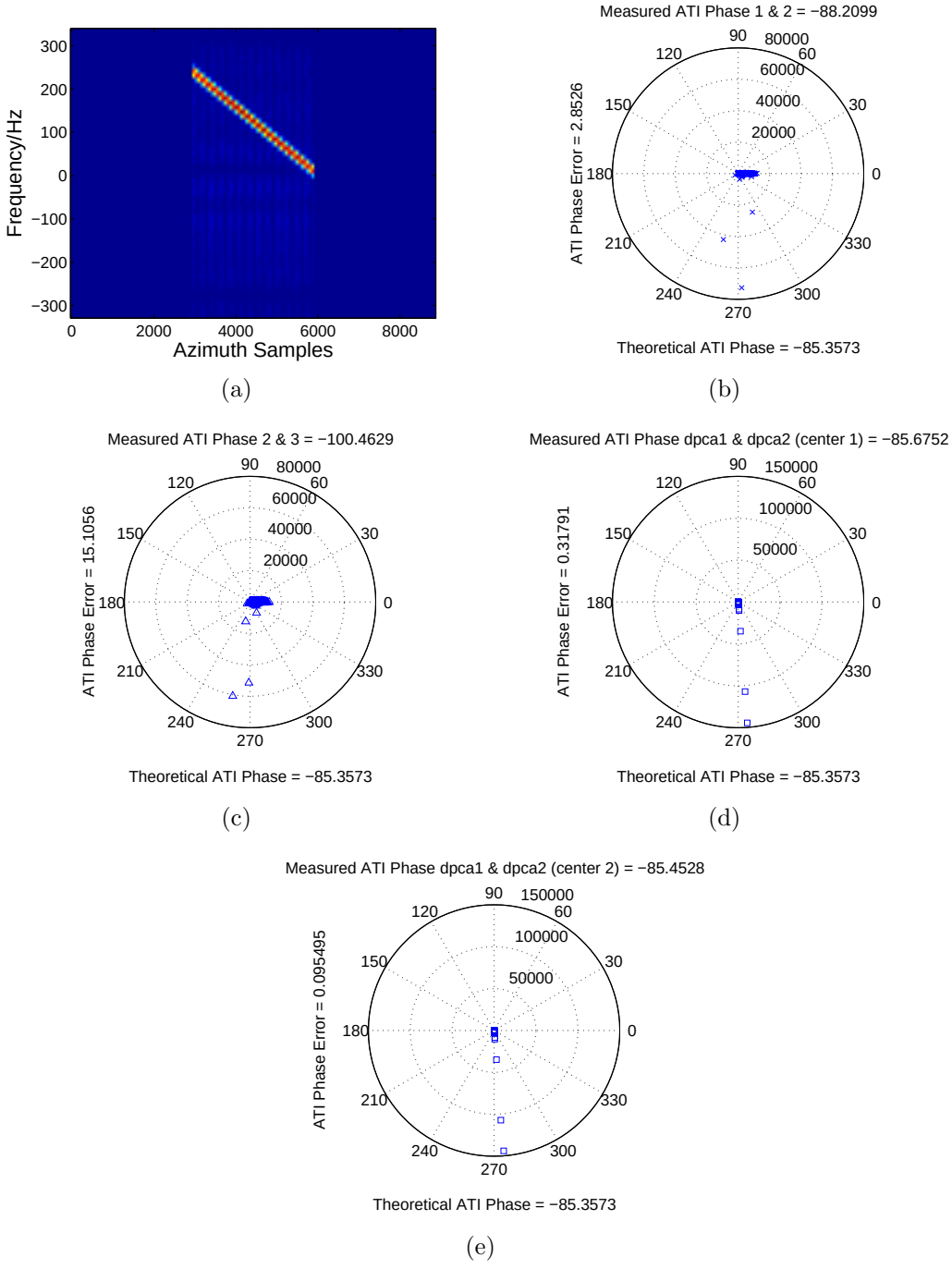

Figure 9: *The same mode as in the previous figure. (a) Time-frequency plots of fore channel minus aft channel and polar plots of interferogram between (b) fore and centre 1 channels, (c) centre 1 and aft channels, (d) DPCA of fore and centre 1 channels and DPCA of centre 1 and aft channels, and (e) DPCA of fore and centre 2 channels and DPCA of centre 2 and aft channels.*

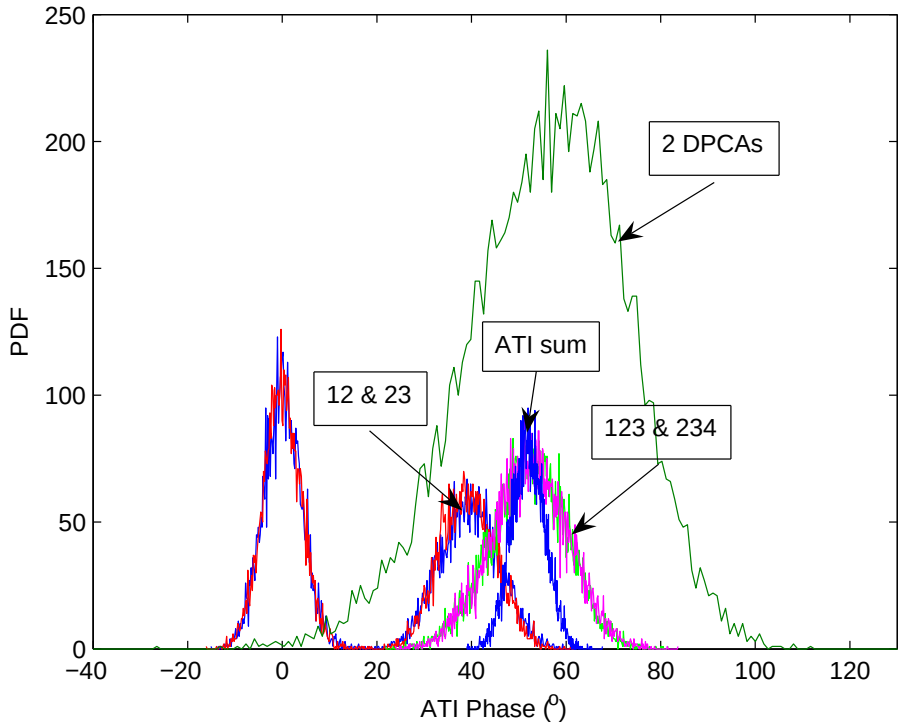

Figure 10: *ATI phase PDFs for two, three, and four channel systems.*

steps:

$$\begin{aligned} DPCA123 &= DPCA12 - DPCA23, \\ DPCA234 &= DPCA23 - DPCA34, \\ ATI &= (DPCA123)(DPCA234)^*, \end{aligned} \tag{9}$$

where $DPCA12$, $DPCA23$, and $DPCA34$ are output signals obtained by subtracting signals between channels 1 and 2, channels 2 and 3, and channels 3 and 4, respectively. As can been in the figure (labelled as '2 DPCAs'), the ATI phase computed in this manner shows a slight bias in the phase measurement and a significantly larger variance. It is clear that this is not the way to compute the ATI phase. There are other ways of computing the ATI phase using the four channels available to us. However, they are not explored further in this Technical Memorandum (further information is included in "spacePDFgenerate_dpca.m" in Appendix D).

The accuracy of ATI phase measurements directly impacts estimation of the target parameters. But how does increasing the number of channels improve the probability of detection? This question can be examined from the perspective of simple DPCA clutter cancellation. In the following, we compare the signal-to-clutter ratio PDFs for

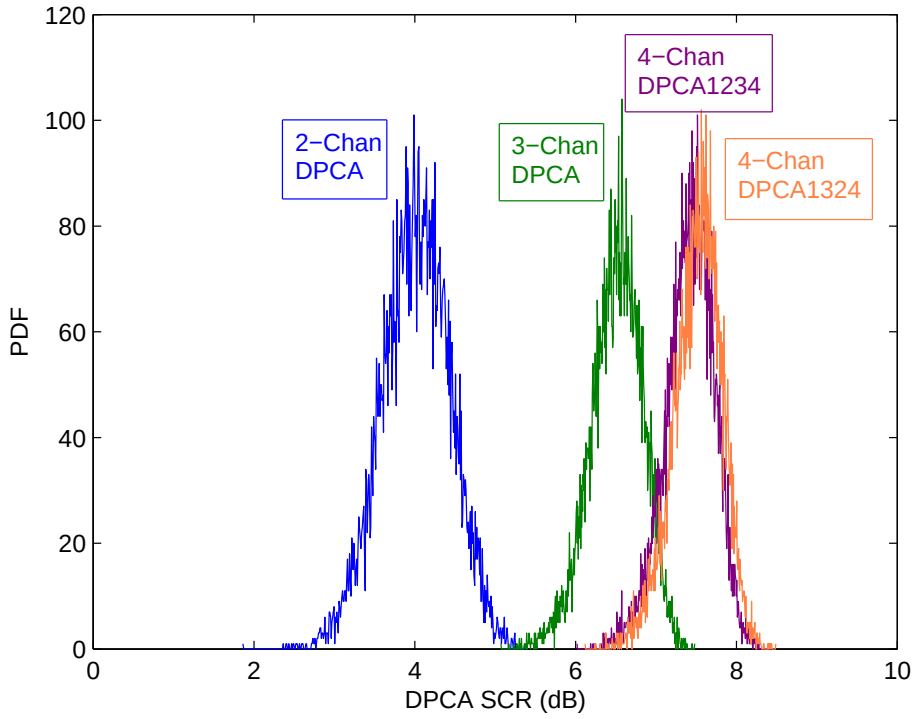

Figure 11: *DPCA signal magnitudes for two, three, and four channel systems.*

two, three and four channel SAR. It is possible to cancel the clutter via DPCA using various combinations of DPCA substraction afforded by the multiple channels. The first is the conventional two-channel approach, which is to subtract one channel from the other co-registered channel to cancel clutter. The second uses three channels to form two DPCAs: one from channels 1 and 2 and the other from channel 2 and 3. Then the two DPCA outputs are coherently added. The third approach uses all four channels to form DPCAs by subtracting channels 1 and 2, channels 2 and 3, and channels 3 and 4. Then all three DPCA outputs are coherently added. Similarly, the fourth approach uses all four channels, but instead of forming DPCA using the neighboring channels, the DPCAs are computed by subtracting channels 1 and 3 and channels 2 and 4. These are then coherently added together to form a new DPCA output. The resulting SCR PDFs for the above four approaches are shown in Fig. 11. As expected, the SCR increases with increasing number of channels. It is interesting to observe that there is a slight variation between SCR PDFs for the third and fourth approaches. It is not clear at the present time why this is so.

5.3.2 Three-Channel Toggle-Receive Mode

A moving target embedded in background stationary clutter is simulated for the three-channel toggle-receive mode, as illustrated in Fig. 5. Shown in Figs. 12(b) through 13(a) are time-frequency representations of signals from the fore channel, the fore channel minus the centre channel, the centre channel minus the aft channel, and the fore channel minus the aft channel. Clearly, clutter cancellation via the virtual channel DPCA subtraction is demonstrated in this three-channel toggle-receive mode. Polar plots of interferograms between the fore and centre channels, the centre and aft channels, and the DPCA of the fore and centre channels and the DPCA of the centre and aft channels are also shown in Figs. 13(b) through 13(d). Interferograms derived from channels without prior clutter cancellation show phase contamination as in Figs. 13(b) and 13(c). The virtual centre channel is again demonstrated to be useful in clutter suppression as seen in Fig. 13(d) in which the interferogram is cleared of clutter contaminants.

5.3.3 Four-Channel Toggle-Receive Mode

Simulation results for the four-channel toggle-receive mode are shown in Figs. 14(a) through 14(f). They are similar to the three-channel toggle-transmit and toggle-receive modes. The results show no surprises. Virtual channels generated from sub-aperture switching or toggling are again shown to be effective in clutter suppression as seen in Figs 14(c) through 14(f) and do indeed improve the interferogram estimation accuracy as shown in Figs. 15(a) through 15(e). The number of degrees of freedom or spatial diversity required to carry out true multi-channel processing of moving targets is indeed increased via the proposed sub-aperture toggling schemes.

6 Conclusions

This Technical Memorandum proposes and describes three multi-channel GMTI modes for the RADARSAT-2 MODEX. The multi-channel concepts make use of the so-called aperture switching or toggling technique, which generates independent phase centres and increases the spatial diversity of a two-physical-channel radar to become a three or four virtual-channel radar. Simulation experiments are conducted to demonstrate the feasibility of such a multi-channel radar system. Results clearly show that virtual channels can be exploited to improve signal-to-clutter ratio (and, therefore, the detection performance), suppress the interfering clutter, and enhance the target parameter estimation accuracy. Other considerations, however, need to be taken into account when applying the technique such as a reduced range swath, beam broadening, and clutter band aliasing.

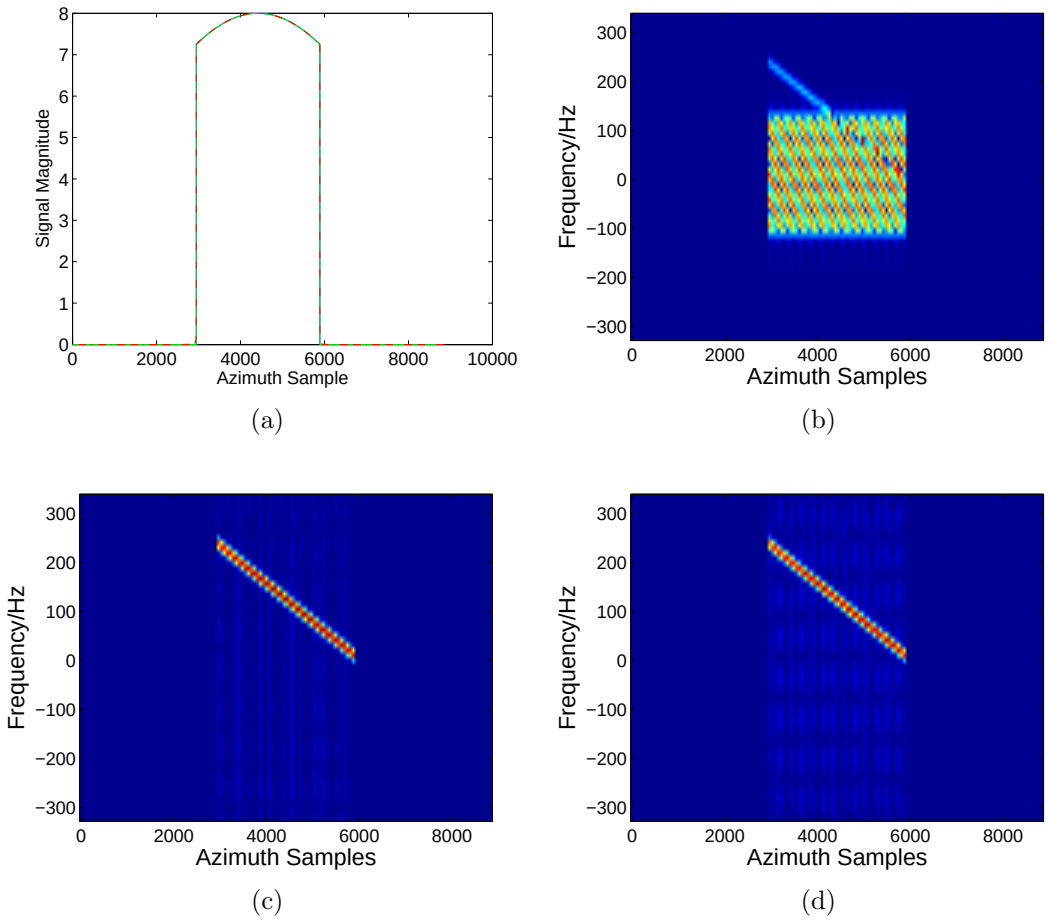

Figure 12: *Three-channel GMTI in toggle-receive mode with a doubling of the PRF. The fore aperture consists of first eight sub-panels of the antenna, the centre aperture consists of the centre eight sub-panels, and the aft aperture consists of the last eight sub-panels. (a) Normalized antenna patterns. Time-frequency plots of (b) fore aperture signal, (c) fore channel minus centre channel, and (d) centre channel minus aft channel.*

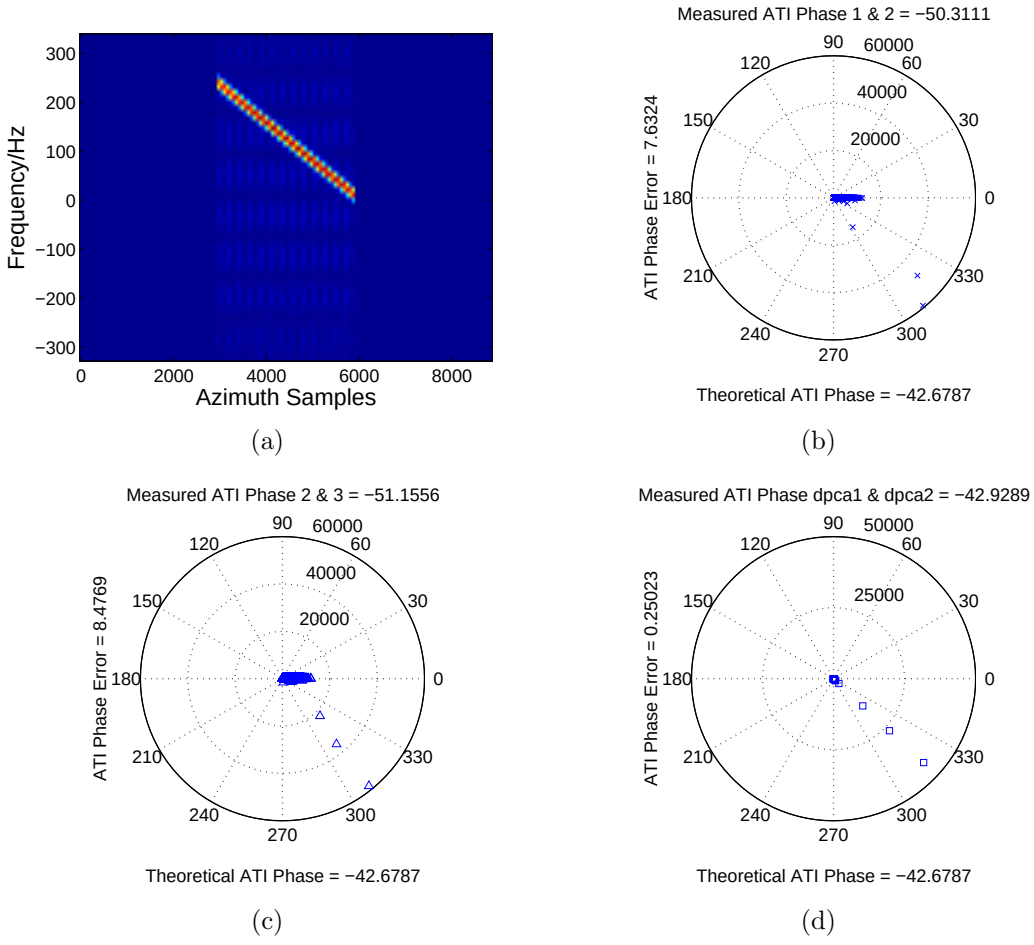

Figure 13: *The same mode as the previous figure. (a) Time-frequency plot of fore channel minus aft channel. Polar plots of the interferogram between (b) fore and centre channels, (c) centre and aft channels, and (d) DPCA of fore and centre channels and DPCA of centre and aft channels.*

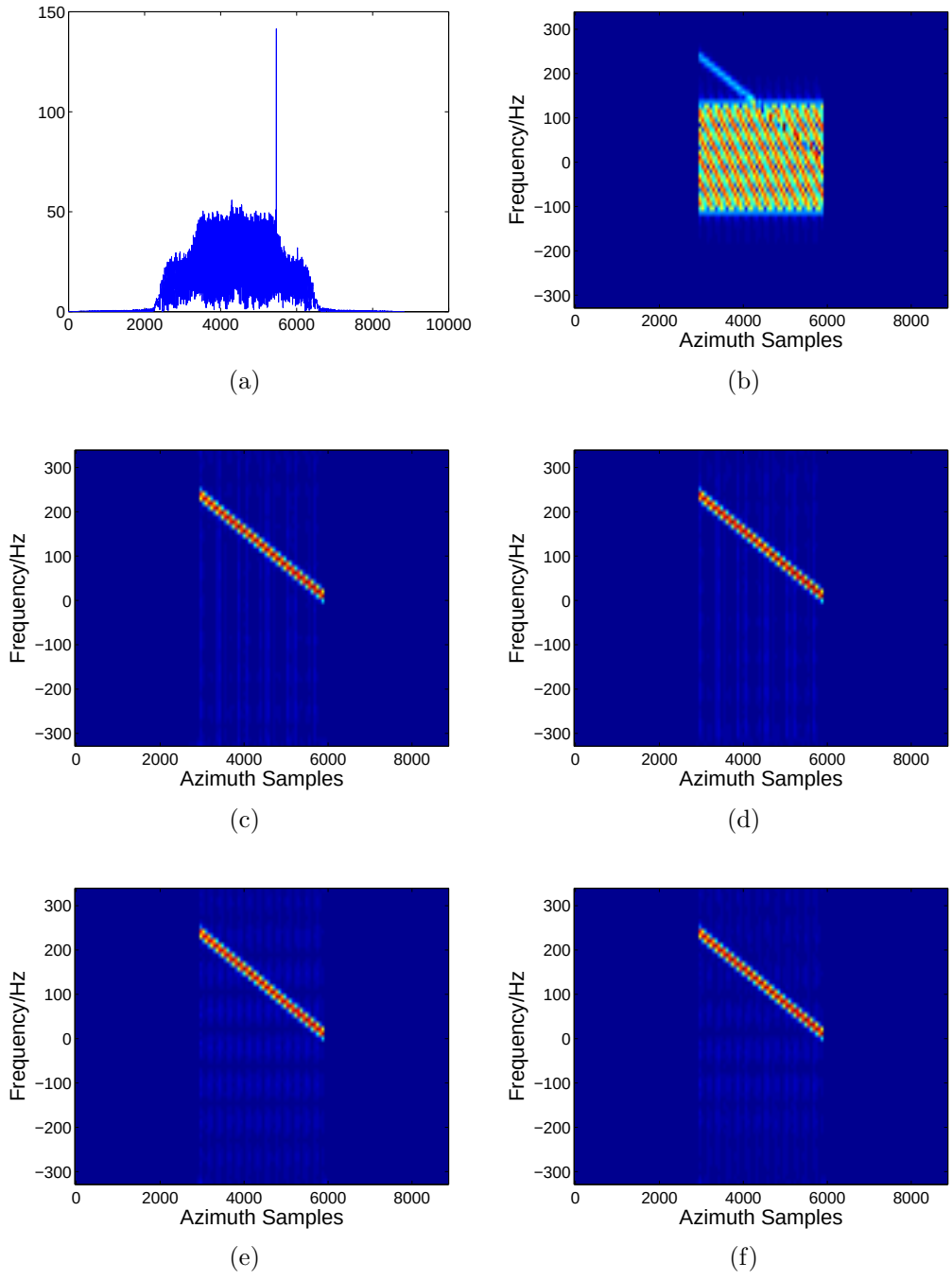

Figure 14: *Four-channel GMTI in toggle-receive mode with a doubling of the PRF: transmit at full aperture and receive at first and third quarter sub-apertures on odd pulses and receive at second and fourth quarter sub-apertures on even pulses. (a) Channel 1 signal magnitude (target plus clutter) after fractional Fourier transform compression, time-frequency plots of (b) channel 1 signal, (c) channel 1 minus channel 2, (d) channel 3 minus channel 4, and (f) channel 1 minus channel 3.*

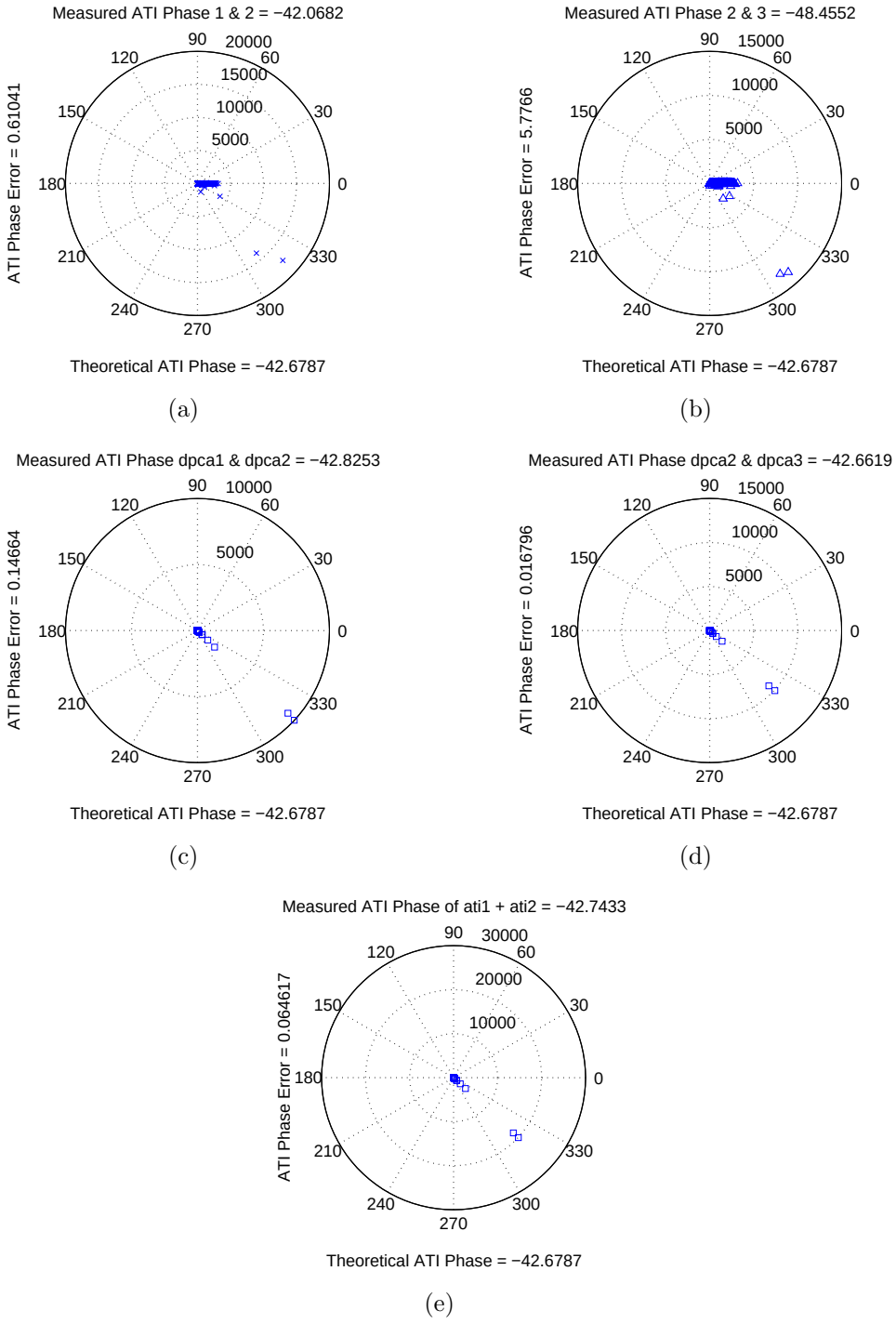

Figure 15: *The same mode as Fig. 15. Polar plots of the phase and amplitude of the interferogram between (a) channels 1 and 2, (b) channels 2 and 3, (c) DPCA of channels 1 and 2 and DPCA of channels 2 and 3, (d) DPCA of channels 2 and 3 and DPCA of channels 3 and 4, and (e) by adding (c) and (d).*

References

[1] Cumming, I.G. and Wong, F.H. 2005. "Digital Processing of Synthetic Aperture Radar Data," Artech House, Boston, 2005, p. 140.

[2] Livingstone, C.E. 1998. The addition of MTI modes to commercial SAR satellites. *Proceedings of 10th CASI Conference on Astronautics*, Ottawa, Canada, 26-28 October 1998, pp. 267-275.

[3] Gierull, C.H. and Sikaneta, I.C. 2003. Raw data based two-aperture SAR ground moving target indication. In IGARSS'2003, *Proceedings of the International Geoscience and Remote Sensing Symposium*, Toulouse, France, 21-25 July.

[4] Stockburger, E.F. and Held, D.N. 1995. Interferometric moving ground target imaging. *The Record of the IEEE 1995 International Radar Conference*, pp. 438-443.

[5] Yadin, E. 1996. A performance evaluation model for a two port interferometer SAR-MTI. *Proceedings of the 1996 IEEE National Radar Conference*, pp. 261-266.

[6] Ender, J.H.G. 1999. Space-time processing for multichannel synthetic aperture radar. Electronics & Communication Engineering Journal, Vol. 11, No. 1, pp. 29-38.

[7] Ender, J.H.G. 1994. Signal processing for multi-channel SAR applied to the experimental SAR system AER. *Proceedings of International Radar Conference*, Paris, May 1994.

[8] Ender, J.H.G., Cerutti-Maori, D., and Bürger, W. 2005. Radar antenna architectures and sampling strategies for space-based moving target recognition, *Proceedings of IGARSS'05*, Seoul, July 2005.

[9] Runge, H., Laux, C, Gabele, M. and Metzig, R. 2006. Performance Analysis of virtual multi-channel modes for TerraSAR-X. *Proceedings of EUSAR'06*, Dresden, Germany, May 2006.

[10] Livingstone, C.E. and Thompson, A.A. 2004. The moving object detection experiment on RADARSAT-2. Can. J. Remote Sensing, Vol. 30, No. 3, pp. 355-368.

[11] Coe, D.J. and White, R.G. 1995. Moving target detection in SAR imagery: experimental results. *The Record of the IEEE 1995 International Radar Conference*, pp. 644-649.

[12] Raney, R.K. 1971. Synthetic aperture imaging radar and moving targets. IEEE Transactions on Aerospace and Electronic Systems, Vol. 7, No. 3, pp. 499-505.

[13] Gierull, C. H. and Livingstone, C. 2004. SAR-GMTI concept for RADARSAT-2, in *The Applications of Space-Time Processing*, R. Klemm, Ed. IEE Press, Stevenage, UK.

[14] Sikaneta, I. C. and Chouinard, J.-Y. 2004. Eigendecomposition of the multi-channel covariance matrix with applications to SAR-GMTI, Signal Processing, Vol. 84, No. 9 (Special Issue), pp. 1501–1535.

[15] Gierull, C. H. 2004. Statistical analysis of multilook SAR interferograms for CFAR detection of ground moving targets, IEEE Trans. Geosci. Remote Sensing, Vol. 42, No. 4, pp. 691–701.

[16] Gierull, C. H. 2002. Moving target detection with along-track SAR interferometry - a theoretical analysis, (DRDC Ottawa TR 2002-084), Defence R&D Canada - Ottawa.

[17] Livingstone, C.E., Sikaneta, I., Gierull, C.H., Chiu, S., Beaudoin, A., Campbell, J., Beaudoin, J., Gong, S., and Knight, T.A. 2002. An airborne SAR experiment to support RADARSAT-2 GMTI. Can. J. Remote Sensing, Vol. 28, No. 6, pp. 794-813.

[18] Chiu, S. 2004. Two-channel SAR-GMTI via fractional Fourier transform, (DRDC Ottawa TM 2004-172), Defence R&D Canada - Ottawa.

[19] Chiu, S. 2005. Application of fractional Fourier Transform to moving target indication via along-track interferometry. EURASIP Journal on Applied Signal Processing, in Special Issue on "Advances in Interferometric Synthetic Aperture Radar Processing," Vol. 2005, No. 20, pp. 3293-3303.

[20] Almeida, L.B. 1994. The fractional Fourier transform and time-frequency representations. IEEE Trans. Signal Processing, Vol. 42, No. 11, pp. 3084-3091.

[21] Zayed, A.I. 1996. On the relationship between the Fourier and fractional Fourier transforms. IEEE Trans. Signal Processing Letters, Vol. 3, No. 12, pp. 310-311.

[22] Dickey, F.R. and Jr., Santa, M.M. 1953. Final report on anticlutter techniques, General Electric Company Report. R65EMH37, 1 March.

[23] Chiu, S. 2003. Clutter effects on ground moving target velocity estimation with SAR along-track interferometry. *Proceedings of IGARSS'2003*, Toulouse, France, 21-25 July.

[24] Sharma, J.J. and Collins, M.J. 2004. Focusing accelerating ground moving targets in SAR imagery. *Proceedings of EUSAR'2004*, Ulm, Germany, 25-27 May.

Annex A: Platform-Motion-Induced Clutter Doppler Spread

There has been discussion in DRDC-Ottawa Space-Based Radar Group about the correct way to compute the clutter Doppler bandwidth for the space-based radar geometry. It was argued that a radar's beam sweeps the ground at slightly lower velocity than the spacecraft. This is given by $v_g = w_s R_e$, where w_s is the platform orbital angular velocity and R_e is the earth's average radius, and therefore induced a correspondingly lower clutter bandwidth. As will be shown below, this argument is erroneous and the platform-motion-induced clutter Doppler spread in space geometry (or spherical geometry) is no different from the airborne flat-earth case, which is simply given by [1]

$$\Delta f_D = 2 f_D = 2\left(2\frac{v_r}{\lambda}\right) = 4\frac{v_s \sin\varphi}{\lambda}, \tag{A.1}$$

where v_s and v_r are the spacecraft velocity and the radial component of this velocity, respectively, 2φ is 3-dB beamwidth angle, λ is wavelength, and zero-angle beam squint is assumed.

To show that the platform-motion induced Doppler spread is independent of the imaging geometry, the above expression can be derived for the spaceborne geometry. Given the imaging geometry as shown in Fig. A.1, the distance between the radar and a scatterer on earth at the edge of the 3-dB antenna main beam (in azimuth) is given by the Law of Cosines

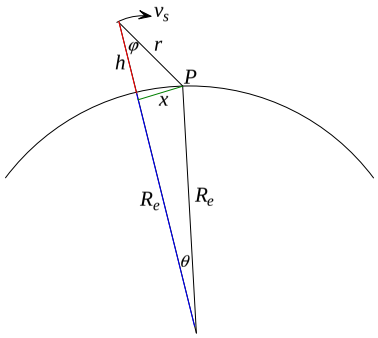

Figure A.1: *Spaceborne geometry for clutter bandwidth calculation.*

as

$$r^2 = R_e^2 + (h + R_e)^2 - 2R_e(h + R_e)\cos\theta. \tag{A.2}$$

Taking the derivative of both sides of (A.2) with respect to time t yields

$$r\frac{\mathrm{d}r}{\mathrm{d}t} = R_e(h + R_e)\sin\theta\frac{\mathrm{d}\theta}{\mathrm{d}t}. \tag{A.3}$$

Therefore, the relative (or radial) velocity $v_r = \mathrm{d}r/\mathrm{d}t$ of a scatterer on earth at the edge of the 3-dB main beam with respect to the radar (ignoring earth motion) is given by

$$v_r = \frac{R_e\omega_s(h + R_e)\sin\theta}{r} = \frac{R_e v_s \sin\theta}{r} = v_s \sin\varphi, \tag{A.4}$$

which is exactly the same expression for v_r as given in (A.1).

Annex B: Taylor Series Expansion of Radar-to-Target Range History

In this section, the range history from radar to a target with constant acceleration is approximated using Taylor series expansion. The details of the derivation are given. Starting with the radar-to-target flat-earth geometry given in Fig. 3, we derive the range history equation:

$$R(t) = \sqrt{[x_0 + (v_{x0} - v_a)t + a_{x0}t^2/2]^2 + [y_0 + v_{y0}t + a_{y0}t^2/2]^2 + h^2}, \tag{B.1}$$

where v and a are target velocity and acceleration, respectively. The subscript "0" denotes values at $t = 0$, and x and y are the along-track and across-track components, respectively. The '0' subscript is retained for acceleration components, though they are assumed to be constant. The target velocity and position at broadside time t_b are therefore

$$\begin{aligned} v_{xb} &= v_{x0} + a_{x0}t_b, \\ v_{yb} &= v_{y0} + a_{y0}t_b, \\ x_b &= v_a t_b = x_0 + v_{x0}t_b + a_{x0}t_b^2/2, \\ y_b &= y_0 + v_{y0}t_b + a_{y0}t_b^2/2. \end{aligned} \tag{B.2}$$

The second last equation of (3) is a result of the definition of "broadside," where the azimuth position of the radar coincides with that of the moving target.

The first derivative of (B.1) can be shown to be

$$\dot{R}(t) = \frac{[x_0 + (v_{x0} - v_a)t + a_{x0}t^2/2][(v_{x0} - v_a) + a_{x0}t] + [y_0 + v_{y0}t + a_{y0}t^2/2][v_{y0} + a_{y0}t]}{\sqrt{[x_0 + (v_{x0} - v_a)t + a_{x0}t^2/2]^2 + [y_0 + v_{y0}t + a_{y0}t^2/2]^2 + h^2}} \tag{B.3}$$

From the second last equation of (B.2), $-x_0 = (v_{x0} - v_a)t_b + a_{x0}t_b^2/2$. Substituting '$-x_0$' and '$y_b$' into and evaluating (B.3) at $t = t_b$ yields

$$\dot{R}(t_b) = \frac{y_b(v_{y0} + a_{y0}t_b)}{R_b} = \gamma v_{yb}, \tag{B.4}$$

where $R_b = R(t_b) = \sqrt{y_b^2 + h^2}$ and $\gamma = y_b/R_b$.

The second derivative of (B.1) can be similarly derived:

$$\begin{aligned}\ddot{R}(t) = &- \frac{\{[x_0 + (v_{x0} - v_a)t + a_{x0}t^2/2][(v_{x0} - v_a) + a_{x0}t] + [y_0 + v_{y0}t + a_{y0}t^2/2][v_{y0} + a_{y0}t]\}^2}{\{[x_0 + (v_{x0} - v_a)t + a_{x0}t^2/2]^2 + [y_0 + v_{y0}t + a_{y0}t^2/2]^2 + h^2\}^{3/2}} \\ &+ \frac{\{[(v_{x0} - v_a) + a_{x0}t]^2 + [x_0 + (v_{x0} - v_a)t + a_{x0}t^2/2]a_{x0} + [v_{y0} + a_{y0}t]^2 + [y_0 + v_{y0}t + a_{y0}t^2/2]a_{y0}\}}{\{[x_0 + (v_{x0} - v_a)t + a_{x0}t^2/2]^2 + [y_0 + v_{y0}t + a_{y0}t^2/2]^2 + h^2\}^{1/2}}.\end{aligned} \tag{B.5}$$

Evaluating $\ddot{R}(t)$ at t_b gives

$$\begin{aligned}\ddot{R}(t_b) = &- \frac{[(y_0 + v_{y0}t_b + a_{y0}t_b^2/2)(v_{y0} + a_{y0}t_b)]^2}{[(y_0 + v_{y0}t_b + a_{y0}t_b^2/2)^2 + h^2]^{3/2}} \\ &+ \frac{[(v_{x0} - v_a) + a_{x0}t_b]^2 + [v_{y0} + a_{y0}t_b]^2 + [y_0 + v_{y0}t_b + a_{y0}t_b^2/2]a_{y0}}{[(y_0 + v_{y0}t_b + a_{y0}t_b^2/2)^2 + h^2]^{1/2}},\end{aligned} \tag{B.6}$$

and substituting v_{xb}, v_{yb}, y_b from (B.2) and R_b into (B.6) finally yields

$$\begin{aligned}\ddot{R}(t_b) = &-\frac{y_b^2 v_{yb}^2}{R_b^3} + \frac{(v_{xb} - v_a)^2 + v_{yb}^2 + y_b a_{y0}}{R_b} \\ = &\frac{1}{R_b}[v_{rel}^2 + y_b a_{y0}],\end{aligned} \tag{B.7}$$

where $v_{rel}^2 = (v_{xb} - v_a)^2 + v_{yb}^2(1 - \gamma^2)$ and $\gamma = y_b/R_b$.

The third derivative of $R(t)$ can now be derived:

$$\begin{aligned}
\dddot{R}(t) = &+ 3\frac{\{[x_0 + (v_{x0} - v_a)t + a_{x0}t^2/2][(v_{x0} - v_a) + a_{x0}t] + [y_0 + v_{y0}t + a_{y0}t^2/2][v_{y0} + a_{y0}t]\}^3}{\{[x_0 + (v_{x0} - v_a)t + a_{x0}t^2/2]^2 + [y_0 + v_{y0}t + a_{y0}t^2/2]^2 + h^2\}^{5/2}} \\
&- 2\{[(v_{x0} - v_a) + a_{x0}t]^2 + [x_0 + (v_{x0} - v_a)t + a_{x0}t^2/2]a_{x0} + [v_{y0} + a_{y0}t]^2 + [y_0 + v_{y0}t + a_{y0}t^2/2]a_{y0}\} \\
&\times \frac{\{[x_0 + (v_{x0} - v_a)t + a_{x0}t^2/2][(v_{x0} - v_a) + a_{x0}t] + [y_0 + v_{y0}t + a_{y0}t^2/2][v_{y0} + a_{y0}t]\}}{\{[x_0 + (v_{x0} - v_a)t + a_{x0}t^2/2]^2 + [y_0 + v_{y0}t + a_{y0}t^2/2]^2 + h^2\}^{3/2}} \\
&- \{[x_0 + (v_{x0} - v_a)t + a_{x0}t^2/2][(v_{x0} - v_a) + a_{x0}t] + [y_0 + v_{y0}t + a_{y0}t^2/2](v_{y0} + a_{y0}t)\} \\
&\times \frac{\{[(v_{x0} - v_a) + a_{x0}t]^2 + [x_0 + (v_{x0} - v_a)t + a_{x0}t^2/2]a_{x0} + [v_{y0} + a_{y0}t]^2 + [y_0 + v_{y0}t + a_{y0}t^2/2]a_{y0}\}}{\{[x_0 + (v_{x0} - v_a)t + a_{x0}t^2/2]^2 + [y_0 + v_{y0}t + a_{y0}t^2/2]^2 + h^2\}^{3/2}} \\
&+ \frac{\{2[(v_{x0} - v_a) + a_{x0}t]a_{x0} + [(v_{x0} - v_a) + a_{x0}t]a_{x0} + 2[v_{y0} + a_{y0}t]a_{y0} + [v_{y0} + a_{y0}t]a_{y0}\}}{\{[x_0 + (v_{x0} - v_a)t + a_{x0}t^2/2]^2 + [y_0 + v_{y0}t + a_{y0}t^2/2]^2 + h^2\}^{1/2}}.
\end{aligned} \tag{B.8}$$

Using again the relationships in (B.2) and evaluating (B.8) at $t = t_b$ leads to

$$\begin{aligned}
\dddot{R}(t_b) &= 3\frac{y_b^3 v_{yb}^3}{R_b^5} - 3\frac{y_b v_{yb}[(v_{xb} - v_a)^2 + v_{yb}^2 + y_b a_{y0}]}{R_b^3} + 3\frac{(v_{xb} - v_a)a_{x0} + v_{yb}a_{y0}}{R_b} \\
&= \frac{3}{R_b}\left\{ v_{yb}a_{y0}(1 - \gamma^2) + (v_{xb} - v_a)a_{x0} - \frac{y_b v_{yb}[(v_{xb} - v_a)^2 + v_{yb}^2]}{R_b^2} + \frac{y_b^3 v_{yb}^3}{R_b^4} \right\} \\
&\approx \frac{3}{R_b}\{v_{yb}a_{y0}(1 - \gamma^2) + (v_{xb} - v_a)a_{x0}\},
\end{aligned} \tag{B.9}$$

where the last two terms, which are negligible, are dropped in the approximation.

The general Taylor series expansion formula (about t_b) is given by

$$R(t) = R(t_b) + \frac{1}{1!}\dot{R}(t_b)(t - t_b) + \frac{1}{2!}\ddot{R}(t_b)(t - t_b)^2 + \frac{1}{3!}\dddot{R}(t_b)(t - t_b)^3 + \cdots . \tag{B.10}$$

Therefore, the final Taylor series expansion representation of (B.1) is

$$R(t) \approx R_b + v_{yb}\gamma(t - t_b) + \frac{1}{2R_b}(v_{rel}^2 + y_b a_{y0})(t - t_b)^2 + \frac{1}{2R_b}[(v_{xb} - v_a)a_{x0} + v_{yb}a_{y0}(1 - \gamma^2)](t - t_b)^3. \tag{B.11}$$

This page intentionally left blank.

Annex C: MATLAB Code 'beamForming2.m'

This MATLAB routine computes two-way antenna patterns for various combinations of transmit and receive antenna sizes.

```
clear all

N = 320;
lambda = 0.0555;
delta_x = 0.815*lambda;
theta = -pi/2:pi/11520:pi/2;
phi_n = 0;

Et = repmat(0,1,length(theta));
for n = 1:N/2
    Et = exp(-j*(2*pi*n*delta_x*sin(theta)/lambda-phi_n)) + Et;
end

Er = repmat(0,1,length(theta));
for m = 1:N/2
    Er = exp(-j*(2*pi*m*delta_x*sin(theta)/lambda-phi_n)) + Er;
end

elemPattern = cos((-(length(Et)-1)/2:1:(length(Et)-1)/2)*pi/(length(Et)-1));
%elemPattern = 1;

Et = elemPattern.*Et;
Er = elemPattern.*Er;
EE_maxdB = 10*log10(max(abs(Et.*Er)));
figure; plot(theta*180/pi,10*log10(abs(Et.*Er)) - EE_maxdB)
xlabel('Angle (degree)'); ylabel('Amplitude (dB)')
```

This page intentionally left blank.

Annex D: MATLAB Code 'spacePDFgenerate_dpca.m'

This MATLAB routine computes magnitude PDFs of DPCA outputs for various combinations of subtracting and adding signals from different channels.

```
clear all

%parameters
simClut = 1;
inv_scr = 8;
plotHist = 0;

%constants
G = 6.67e-11; %gravitational constant
Me = 5.98e24; %mass of the Earth
Re = 6372.795477598e3; %quadratic mean radius of the Earth
hs = 800e3; %spacecraft altitute
Rs = Re + hs; %spacecraft orbital radius
c = 3e8; %speed of light

%geometry parameters
incTheta = 50*pi/180; %angle of incidence
phi = asin((Re/(Re+hs))*sin(incTheta)); %angle of depression
psi = incTheta-phi; %look angle
ws = sqrt((G*Me)/Rs^3); %spacecraft angle velocity
r0 = Rs*sin(psi)/sin(incTheta); %slant range at time zero

%target parameters with earth motions
vtx = -10;
vtr = 15;
vex = -32.3766; %calculated from orbital paramters
ver = 269.5196; %calculated from orbital parameters
vx = vtx + vex;
vr = vtr + ver;
```

```
delta_x0 = -100; %this number should NOT be too large or else approximation breaks down !!!
tb = delta_x0/(Rs*ws-vx); %this is a negligible approximation

%spacecraft parameters
vsxb = Rs*cos(ws*tb)*ws;
asxb = -Rs*sin(ws*tb)*ws^2;
phi_s = atan(ver/(vsxb-vex));

%relative parameters
x0 = r0*tan(phi_s) + delta_x0;
R0 = sqrt(x0^2 + r0^2); %initial range (at t = 0 )

%radar parameters
fc = 5.405e9; %radar centre frequency
lambda = c/fc;
k = 2*pi/lambda; %wavenumber
fs = 3800/2; %pulse repetition frequency
tpri = 1/fs;
d = 7.5/4; %distance between phase centres
D = d*cos(phi_s); %true DPCA distance in along-track direction
tdpca = D/vsxb;
shift_incr = tdpca/tpri;

%generate time vector t and antenna gain pattern b
delta_t = -0.2;
Theta = 0.38; %azimuth beamwidth in degree
theta = Theta*pi/180; %convert degree beamwidth to radian beamwidth
x = r0*tan(theta/2);
beamWidth = 2*x/vsxb; %beamwidth expressed in time unit
N = 2*13750; %total number of samples
t = -(N-1)/2:(N-1)/2; t = t*tpri;
T = beamWidth-2*abs(delta_t);
b = rectpuls(t-tb-delta_t,T); % true new pulse centre is half of shift in rectpuls
%b = (sinc((t-tb-delta_t)/T)).^2;

%calculate intermediate parameters
```

```
%Rb = sqrt((r0*tan(phi_s) + delta_x0 + vx*tb - Rs*sin(ws*tb))^2 + (r0 + vr*tb - Rs*(1 - cos(ws*tb))*cos(phi))^2)
Rb = sqrt((r0*tan(phi_s))^2 + (r0 + vr*tb - Rs*(1 - cos(ws*tb))*cos(phi))^2);
vsrb = Rs*sin(ws*tb)*ws*cos(phi);
asrb = Rs*cos(ws*tb)*ws^2*cos(phi);
vrel = sqrt((vx - vsxb)^2 + vr^2 - r0*asrb); %note the complete expression yields exactly the same result
%vrel = sqrt((vx - vsxb)^2 + (vr - vsrb)^2 - r0*tan(phi_s)*asxb - r0*asrb)
ve = vrel^2/vsxb + (vx - vsxb);
vr_hat = tan(phi_s)*vtx + vtr;
gamma = r0/Rb;

%generate pulses in slow time
%Channel 1
R1 = sqrt((x0 + vx*t - Rs*sin(ws*t)).^2 + (r0 + vr*t - Rs*cos(phi)*(1-cos(ws*t))).^2);
%R1 = Rb + gamma*vr_hat*(t-tb) + vrel^2*(t-tb).^2/(2*Rb);
%figure; plot(t,R1)
%s1 = b.*exp(-j*4*pi*R1/lambda);
s1o = b.*exp(-j*2*k*R1);

%Channel 2
%The discrepacies between the far field approximation and "exact" equation
%is that in exact approach, the aft aperture is delayed in BOTH azimuth and
%range directions. The question: is this model correct? NO! The aft
%aperture should not be delayed in range direction!
R2 = sqrt((x0 + vx*t - (Rs - d*sin(phi_s))*sin(ws*(t-tdpca))).^2 + (r0 + vr*t ...
    - (Rs*cos(phi)*(1 - cos(ws*t)) + d*sin(phi_s)*cos(ws*t))).^2);
        %*****************************************************************
        %The far-field approximation give the same result as the exact equations
        %xrelb = r0*tan(phi_s) + delta_x0 + vx*t - Rs*sin(ws*t);
        %rrelb = r0 + vr*tb - Rs*cos(phi)*(1-cos(ws*tb));
        %R2 = R1 + D*(vx - vsxb)*(t-tb)/Rb;
        %*****************************************************************
s2u = b.*exp(-j*2*k*R2);
s2o = (shiftM(s2u',-shift_incr))'; %coregistration

%channel 3
R3 = sqrt((x0 + vx*t - (Rs - 2*d*sin(phi_s))*sin(ws*(t-2*tdpca))).^2 + (r0 + vr*t ...
```

```
        - (Rs*cos(phi)*(1 - cos(ws*t)) + 2*d*sin(phi_s)*cos(ws*t))).^2);
s3u = b.*exp(-j*4*pi*R3/lambda);
s3o = (shiftM(s3u',-2*shift_incr))'; %coregistration

%channel 4
R4 = sqrt((x0 + vx*t - (Rs - 3*d*sin(phi_s))*sin(ws*(t-3*tdpca))).^2 + (r0 + vr*t ...
        - (Rs*cos(phi)*(1 - cos(ws*t)) + 3*d*sin(phi_s)*cos(ws*t))).^2);
s4u = b.*exp(-j*4*pi*R4/lambda);
s4o = (shiftM(s4u',-3*shift_incr))'; %coregistration

%calculate theoretical ATI phases
phi_ATI = (k*gamma*vr_hat*2*D/vsxb + k*2*D*ve*delta_t/Rb)*180/pi;



for n = 1:10000
n
%generate Gaussian clutter for each channel
%rho is coherence between channels, e.g. rho=0.95 (could be complex if needed)
rho = 0.95;
Rc = [[1 rho rho rho]; [conj(rho) 1 rho rho]; [conj(rho) conj(rho) 1 rho]; ...
     [conj(rho) conj(rho) conj(rho) 1]]; %covariance matrix
Rc1 = Rc^(0.5);
Zc = 1/sqrt(2)*(randn(4,N)+j*randn(4,N));  % standard complex normal data
clutter = Rc1*Zc;  %size = [4 N]

%add clutter to signals
if simClut ==  1
    s1_clut = inv_scr*clutter(1,:);
    s2_clut = inv_scr*clutter(2,:);
    s3_clut = inv_scr*clutter(3,:);
    s4_clut = inv_scr*clutter(4,:);
    s1 = s1o + s1_clut;
    s2 = s2o + s2_clut;
    s3 = s3o + s3_clut;
    s4 = s4o + s4_clut;
```

```
end

%compute fractional Fourier transforms
alpha = acot(k*vrel^2*N/(pi*Rb*fs^2)); %calculate theoretical alpha
a = alpha/(pi/2);
z1 = fracF(s1,a);
z2 = fracF(s2,a);
z3 = fracF(s3,a);
z4 = fracF(s4,a);
z1_clut = fracF(s1_clut,a);
z2_clut = fracF(s2_clut,a);
z3_clut = fracF(s3_clut,a);
z4_clut = fracF(s4_clut,a);

%compute DPCAs
dpca12 = z1-z2;
dpca23 = z2-z3;
dpca34 = z3-z4;
dpca13 = z1-z3; %this equivalent to 3-channel twice the baseline
dpca24 = z2-z4; %this equivalent to 3-channel twice the baseline

dpca12_clut = z1_clut-z2_clut;
dpca23_clut = z2_clut-z3_clut;
dpca34_clut = z3_clut-z4_clut;
dpca13_clut = z1_clut-z3_clut; %this equivalent to 3-channel twice the baseline
dpca24_clut = z2_clut-z4_clut; %this equivalent to 3-channel twice the baseline

dpcaMag12(n) = max(abs(dpca12));
dpcaMag12_clut(n) = max(abs(dpca12_clut));

DPCA123 = dpca12+dpca23;
dpcaMag123(n) = max(abs(DPCA123));
DPCA123_clut = dpca12_clut+dpca23_clut;
dpcaMag123_clut(n) = max(abs(DPCA123_clut));

DPCA234 = dpca23+dpca34;
```

```
dpcaMag234(n) = max(abs(DPCA234));
DPCA234_clut = dpca23_clut+dpca34_clut;
dpcaMag234_clut(n) = max(abs(DPCA234_clut));

DPCA1234 = dpca12+dpca23+dpca34;
dpcaMag1234(n) = max(abs(DPCA1234));
DPCA1234_clut = dpca12_clut+dpca23_clut+dpca34_clut;
dpcaMag1234_clut(n) = max(abs(DPCA1234_clut));

DPCA1324 = dpca13+dpca24;
dpcaMag1324(n) = max(abs(DPCA1324));
DPCA1324_clut = dpca13_clut+dpca24_clut;
dpcaMag1324_clut(n) = max(abs(DPCA1324_clut));

end %realization loop

save 2005Oct17_DPCAs.mat dpcaMag12 dpcaMag12_clut dpcaMag123 dpcaMag123_clut ...
     dpcaMag234 dpcaMag234_clut dpcaMag1234  dpcaMag1234_clut dpcaMag1324 dpcaMag1324_clut
clear all
```

Annex E: MATLAB Code 'airMultiChan_toggle.m'

```
clear all

%This version ('airMultiChan_toggle') uses toggle mode
%to generate third phase centre
%Modification date: Dec 09, 2005

%constants
R0 = 10928; %initial radar-to-target slant range
h =  6468.729; %platform height
va = 130; %platform velocity
lambda = 0.056564; %transmitter wavelength
PRF_per_va = 5.14; %m^-1
fs = PRF_per_va*va; %pulse repetition frequency
tpri = 1/fs; %pulse repetition interval
D = 2*0.2704; %true physical centre separation

%input parameters
vy0 = -4;
vx0 = 3;
x0 = 0; %initial target x-position [m]
y0 = sqrt(R0^2 - h^2); %initial target y-position [m]
delta_t = 0; %tb error or offset expressed in [s]

%calculated parameters
tb = x0/(va-vx0);
yb = y0 + vy0*tb;
Rb = sqrt(yb^2 + h^2);
beta = 2*pi/lambda;
gamma = yb/Rb;
vrel =sqrt((vx0-va)^2 + (1-gamma^2)*vy0^2);

%Target signal length Ts:
Theta = 3; %3 degree for 3dB beamwidth
```

```
theta = Theta*pi/180; %convert to radians
az = int32(Rb*tan(theta/2)*5.14); %convert beam angle to sample number
az = double(az); %[samples]
Ts = 2*az*tpri; %[s] target signal length
T = 3.005*Ts; %total signal length
t1 = -(T-tpri)/2:tpri:(T-tpri)/2; %odd pulses
t2 = -(T-2*tpri)/2:tpri:T/2; %even pulses

%generate transmit signal range history
m = -15:2:15;
t1_mat = repmat(t1',[1 length(m)]);
m1_mat = repmat(m,[length(t1) 1]);
x1_mat = x0 + vx0*t1_mat;
y1_mat = y0 + vy0*t1_mat;
Rt1 = sqrt( (x1_mat - (va*t1_mat + 8*D/16)).^2 + y1_mat.^2 + h^2 ); %transmit range history
Rr1 = sqrt( (x1_mat - (va*t1_mat - m1_mat*D/16)).^2 + y1_mat.^2 + h^2 ); %receive range history
s1 = rectpuls(t1_mat - (tb + delta_t),Ts).*exp(-j*beta*(Rt1 + Rr1));

t2_mat = repmat(t2',[1 length(m)]);
m2_mat = repmat(m,[length(t2) 1]);
x2_mat = x0 + vx0*t2_mat;
y2_mat = y0 + vy0*t2_mat;
Rt2 = sqrt( (x2_mat - (va*t2_mat - 8*D/16)).^2 + y2_mat.^2 + h^2 ); %transmit range history
Rr2 = sqrt( (x2_mat - (va*t2_mat - m2_mat*D/16)).^2 + y2_mat.^2 + h^2 ); %receive range history
s2 = rectpuls(t2_mat - (tb + delta_t),Ts).*exp(-j*beta*(Rt2 + Rr2));

%sub-aperture assignment
m1 = 1:8; %fore or centre sub-apertures
m2 = 9:16; %centre or aft sub-apertures

%generate sub-apertures
sf = sum(s1(:,m1),2);
sc1 = sum(s1(:,m2),2); sc1r = shiftM(sc1,-((8*D/16)/va)/tpri);
sc2 = sum(s2(:,m1),2); sc2r = shiftM(sc2,-((8*D/16)/va)/tpri + 1/2); %sc1r = sc2r;
sa = sum(s2(:,m2),2); sar = shiftM(sa,-((16*D/16)/va)/tpri + 1/2);
```

```
% %alternate way of performing dpca
% dpcafc1r = sf - sc1r; tfPlotSig(dpcafc1r,fs)
% dpcac2ra = shiftM(sc2,((8*D/16)/va)/tpri) - sa; %register centre 2 aperture with aft aperture and perform dpca
% tfPlotSig(dpcac2ra,fs)
% dpcac2rar = shiftM(dpcac2ra,-((16*D/16)/va)/tpri + 1/2);
% tfPlotSig(dpcac2rar,fs)

%normalize the antenna pattern magnitudes
ind = find(sf); %find index of nonzero elements in array
magCal = abs(sf(ind))./abs(sc1r(ind));
sc1r(ind)= sc1r(ind).*magCal;
figure; plot(abs(sf)); hold on
plot(abs(sc1),'g-')
plot(abs(sc1r),'r-.'); hold off
xlabel('Azimuth Sample'); ylabel('Signal Magnitude')

%generate clutter signals
xn = (-T/2:50*tpri:T/2)*va;
n = length(xn)
s1_clut = 0;
s2_clut = 0;
for xc = xn
    tb_clut = xc/va;
    Rct1 = sqrt((xc - (va*t1_mat + 8*D/16)).^2 + y0^2 + h^2);
    Rcr1 = sqrt((xc - (va*t1_mat - m1_mat*D/16)).^2 + y0^2 + h^2);
    s1_clut = s1_clut + rectpuls(t1_mat-(tb_clut+delta_t),Ts).*exp(-j*beta*(Rct1+Rcr1));
    n = n-1
    Rct2 = sqrt((xc - (va*t2_mat - 8*D/16)).^2 + y0^2 + h^2);
    Rcr2 = sqrt((xc - (va*t2_mat - m2_mat*D/16)).^2 + y0^2 + h^2);
    s2_clut = s2_clut + rectpuls(t2_mat-(tb_clut+delta_t),Ts).*exp(-j*beta*(Rct2+Rcr2));
end

%generate sub-apertures for clutter signals
sf_clut = rectpuls(t1'-(tb+delta_t),Ts).*sum(s1_clut(:,m1),2);
sc1_clut = rectpuls(t1'-(tb+delta_t),Ts).*sum(s1_clut(:,m2),2); sc1_clutr = shiftM(sc1_clut,-((8*D/16)/va)/tpri);
sc2_clut = rectpuls(t2'-(tb+delta_t),Ts).*sum(s2_clut(:,m1),2); sc2_clutr = shiftM(sc2_clut,-((8*D/16)/va)/tpri+1/2);
```

```
sa_clut = rectpuls(t2'-(tb+delta_t),Ts).*sum(s2_clut(:,m2),2); sa_clutr = shiftM(sa_clut,-((16*D/16)/va)/tpri+1/2);

% %normalize the antenna pattern magnitudes for 2nd aperture clutter
% sc1_clutr(ind)c= sc1_clutr(ind).*magCal; %use the same pattern as target signal
% sc2_clutr(ind) = sc2_clutr(ind).*magCal;

%add target and clutter signals
sf = sf + sf_clut;
sc1 = sc1 + sc1_clut; sc1r = shiftM(sc1,-((8*D/16)/va)/tpri);
sc2 = sc2 + sc2_clut; sc2r = shiftM(sc2,-((8*D/16)/va)/tpri + 1/2); %sc1r = sc2r;
sa = sa + sa_clut; sar = shiftM(sa,-((16*D/16)/va)/tpri + 1/2);

%normalize the resulting signal if necessary
sc1r(ind)= sc1r(ind).*magCal;

%calculate theoretical fractional angle
N = length(t1);
frac_a = (2/pi)*acot(beta*N*vrel^2/(pi*Rb*fs^2));

%calculate theoretical ATI phase
ve = vrel^2/va + (vx0-va);
atiPhase = (beta*(D)*gamma*vy0/va + beta*(D)*ve*delta_t/Rb)*180/pi %toggle mode baseline is D not D/2

%compute fractional Fourier transfors
Sf = fracF(sf,frac_a); figure; plot(abs(Sf))
Sc1r = fracF(sc1r,frac_a); %figure; plot(abs(Sc1r))
Sc2r = fracF(sc2r,frac_a); %figure; plot(abs(Sc2r))
Sar = fracF(sar,frac_a); %figure; plot(abs(Sar))

%time-frequency plot of signals
tfPlotSig(sf,fs)
tfPlotSig(sf-sc1r,fs)
tfPlotSig(sc1r-sar,fs)
tfPlotSig(sc2r-sar,fs)
tfPlotSig(sf-sar,fs)
```

```
%calculate interferograms
ati1 = Sf.*conj(Sc1r);
ati2 = Sc1r.*conj(Sar);
ati3 = (Sf-Sc1r).*conj(Sc1r-Sar);
ati4 = (Sf-Sc2r).*conj(Sc2r-Sar);

figure; polar(angle(ati1),abs(ati1),'x');
[ATImag,J] = max(abs(ati1));
atiPhase_max = angle(ati1(J,1))*180/pi;
title(['Measured ATI Phase 1 & 2 = ', num2str(atiPhase_max)]);
xlabel(['Theoretical ATI Phase = ', num2str(atiPhase)]);
ylabel(['ATI Phase Error = ', num2str(abs(atiPhase-atiPhase_max))]);

figure; polar(angle(ati2),abs(ati2),'^');
[ATImag,J] = max(abs(ati2));
atiPhase_max = angle(ati2(J,1))*180/pi;
title(['Measured ATI Phase 2 & 3 = ', num2str(atiPhase_max)]);
xlabel(['Theoretical ATI Phase = ', num2str(atiPhase)]);
ylabel(['ATI Phase Error = ', num2str(abs(atiPhase-atiPhase_max))]);

figure; polar(angle(ati3),abs(ati3),'square'); [ATImag,J] =
max(abs(ati3)); atiPhase_max = angle(ati3(J,1))*180/pi;
title(['Measured ATI Phase dpca1 & dpca2 (centre 1) = ',
num2str(atiPhase_max)]); xlabel(['Theoretical ATI Phase = ',
num2str(atiPhase)]); ylabel(['ATI Phase Error = ',
num2str(abs(atiPhase-atiPhase_max))]);

figure; polar(angle(ati4),abs(ati4),'square'); [ATImag,J] =
max(abs(ati4)); atiPhase_max = angle(ati4(J,1))*180/pi;
title(['Measured ATI Phase dpca1 & dpca2 (centre 2) = ',
num2str(atiPhase_max)]); xlabel(['Theoretical ATI Phase = ',
num2str(atiPhase)]); ylabel(['ATI Phase Error = ',
num2str(abs(atiPhase-atiPhase_max))]);
```

This page intentionally left blank.

Annex F: MATLAB Code 'airMultiChan_clut3.m'

```
clear all

%This version ('airMultiChan_clut3') uses alternate pulses
%to generate third phase centre
%Modification date: Nov 16, 2005

%constants
R0 = 10928;
h =  6468.729;
va = 130;
lambda = 0.056564;
PRF_per_va = 5.14; %m^-1
fs = PRF_per_va*va;
tpri = 1/fs;
D = 2*0.2704; %true physical centre separation

%input parameters
vy0 = -4;
vx0 = 3;
x0 = 0; %initial target x-position [m]
y0 = sqrt(R0^2 - h^2); %initial target y-position [m]
delta_t = 0; %tb error or offset expressed in [s]

%calculated parameters
tb = x0/(va-vx0);
yb = y0 + vy0*tb;
Rb = sqrt(yb^2 + h^2);
beta = 2*pi/lambda;
gamma = yb/Rb;
vrel =sqrt((vx0-va)^2 + (1-gamma^2)*vy0^2);

%Target signal length Ts:
Theta = 3; %3 degree for 3dB beamwidth
```

```
theta = Theta*pi/180; %convert to radians
az = int32(Rb*tan(theta/2)*5.14); %convert beam angle to sample number
az = double(az); %[samples]
Ts = 2*az*tpri; %[s] target signal length
T = 3.005*Ts; %total signal length
t1 = -(T-tpri)/2:tpri:(T-tpri)/2;
t2 = -(T-2*tpri)/2:tpri:T/2;

%generate transmit signal range history
m = -15:2:15;
t1_mat = repmat(t1',[1 length(m)]);
m1_mat = repmat(m,[length(t1) 1]);
x1_mat = x0 + vx0*t1_mat;
y1_mat = y0 + vy0*t1_mat;
Rt1 = sqrt( (x1_mat - va*t1_mat).^2 + y1_mat.^2 + h^2 ); %transmit range history
Rr1 = sqrt( (x1_mat - (va*t1_mat - m1_mat*D/16)).^2 + y1_mat.^2 + h^2 ); %receive range history
s1 = rectpuls(t1_mat - (tb + delta_t),Ts).*exp(-j*beta*(Rt1 + Rr1));

t2_mat = repmat(t2',[1 length(m)]);
m2_mat = repmat(m,[length(t2) 1]);
x2_mat = x0 + vx0*t2_mat;
y2_mat = y0 + vy0*t2_mat;
Rt2 = sqrt( (x2_mat - va*t2_mat).^2 + y2_mat.^2 + h^2 ); %transmit range history
Rr2 = sqrt( (x2_mat - (va*t2_mat - m2_mat*D/16)).^2 + y2_mat.^2 + h^2 ); %receive range history
s2 = rectpuls(t2_mat - (tb + delta_t),Ts).*exp(-j*beta*(Rt2 + Rr2));

%sub-aperture assignment
m1 = 1:8;
m2 = 1:16;
m3 = 9:16;

%generate sub-apertures
sf = sum(s1(:,m1),2);
sc = sum(s2(:,m2),2); scr = shiftM(sc,-((4*D/16)/va)/tpri+1/2); %need to modify this
sa = sum(s1(:,m3),2); sar = shiftM(sa,-((8*D/16)/va)/tpri);
```

```
%normalize the antenna pattern magnitudes
ind = find(sf); %find index of nonzero elements in array
magCal = abs(sf(ind))./abs(scr(ind));
scr(ind)= scr(ind).*magCal;
figure; plot(abs(sf)); hold on
plot(abs(sc),'g-')
plot(abs(scr),'r-.'); hold off
xlabel('Azimuth Sample'); ylabel('Signal Magnitude')

 %generate clutter signals
 xn = (-T/2:50*tpri:T/2)*va;
 n = length(xn)
 s1_clut = 0;
 s2_clut = 0;
 for xc = xn
     tb_clut = xc/va;
     Rct1 = sqrt((xc - va*t1_mat).^2 + y0^2 + h^2);
     Rcr1 = sqrt((xc - (va*t1_mat - m1_mat*D/16)).^2 + y0^2 + h^2);
     s1_clut = s1_clut + rectpuls(t1_mat-(tb_clut+delta_t),Ts).*exp(-j*beta*(Rct1+Rcr1));
     n = n-1
     Rct2 = sqrt((xc - va*t2_mat).^2 + y0^2 + h^2);
     Rcr2 = sqrt((xc - (va*t2_mat - m2_mat*D/16)).^2 + y0^2 + h^2);
     s2_clut = s2_clut + rectpuls(t2_mat-(tb_clut+delta_t),Ts).*exp(-j*beta*(Rct2+Rcr2));
 end

 %generate sub-apertures for clutter signals
 sf_clut = rectpuls(t1'-(tb+delta_t),Ts).*sum(s1_clut(:,m1),2);
 sc_clut = sum(s2_clut(:,m2),2); sc_clutr = rectpuls(t2'-(tb+delta_t),Ts).*shiftM(sc_clut,-((4*D/16)/va)/tpri+1/2);
 sa_clut = sum(s1_clut(:,m3),2); sa_clutr = rectpuls(t1'-(tb+delta_t),Ts).*shiftM(sa_clut,-((8*D/16)/va)/tpri);

 %normalize the antenna pattern magnitudes for 2nd aperture clutter
 sc_clutr(ind)= sc_clutr(ind).*magCal; %use the same pattern as target signal

%add target and clutter signals
sf = sf + sf_clut;
scr = scr + sc_clutr;
```

```
sar = sar + sa_clutr;

%calculate theoretical fractional angle
N = length(t1);
frac_a = (2/pi)*acot(beta*N*vrel^2/(pi*Rb*fs^2));

%calculate theoretical ATI phase
ve = vrel^2/va + (vx0-va);
atiPhase = (beta*(D/2)*gamma*vy0/va + beta*(D/2)*ve*delta_t/Rb)*180/pi

%compute fractional Fourier transfors
Sf = fracF(sf,frac_a); figure; plot(abs(Sf))
Scr = fracF(scr,frac_a); %figure; plot(abs(S2r))
Sar = fracF(sar,frac_a); %figure; plot(abs(S3r))

%time-frequency plot of signals
tfPlotSig(sf,fs)
tfPlotSig(sf-scr,fs)
tfPlotSig(scr-sar,fs)
tfPlotSig(sf-sar,fs)

%calculate interferograms
ati1 = Sf.*conj(Scr);
ati2 = Scr.*conj(Sar);
ati3 = (Sf-Scr).*conj(Scr-Sar);
ati = Sf.*conj(Sar);

figure; polar(angle(ati1),abs(ati1),'x');
[ATImag,J] = max(abs(ati1));
atiPhase_max = angle(ati1(J,1))*180/pi;
title(['Measured ATI Phase 1 & 2 = ', num2str(atiPhase_max)]);
xlabel(['Theoretical ATI Phase = ', num2str(atiPhase)]);
ylabel(['ATI Phase Error = ', num2str(abs(atiPhase-atiPhase_max))]);

figure; polar(angle(ati2),abs(ati2),'^');
[ATImag,J] = max(abs(ati2));
```

```
atiPhase_max = angle(ati2(J,1))*180/pi;
title(['Measured ATI Phase 2 & 3 = ', num2str(atiPhase_max)]);
xlabel(['Theoretical ATI Phase = ', num2str(atiPhase)]);
ylabel(['ATI Phase Error = ', num2str(abs(atiPhase-atiPhase_max))]);

figure; polar(angle(ati3),abs(ati3),'square');
[ATImag,J] = max(abs(ati3));
atiPhase_max = angle(ati3(J,1))*180/pi;
title(['Measured ATI Phase dpca1 & dpca2 = ', num2str(atiPhase_max)]);
xlabel(['Theoretical ATI Phase = ', num2str(atiPhase)]);
ylabel(['ATI Phase Error = ', num2str(abs(atiPhase-atiPhase_max))]);

figure; polar(angle(ati),abs(ati),'square');
[ATImag,J] = max(abs(ati));
atiPhase_max = angle(ati(J,1))*180/pi;
title(['Measured ATI Phase 1 & 3 = ', num2str(atiPhase_max)]);
xlabel(['Theoretical ATI Phase = ', num2str(atiPhase)]);
ylabel(['ATI Phase Error = ', num2str(abs(atiPhase-atiPhase_max))]);
```

This page intentionally left blank.

Annex G: MATLAB Code 'airMultiChan_fourChan.m'

```
clear all

%This version ('airMultiChan_fourChan') uses alternating pulses
%to generate third  and fourth phase centres
%Modification date: Dec 13, 2005

%constants
R0 = 10928;
h =  6468.729;
va = 130;
lambda = 0.056564;
PRF_per_va = 5.14; %m^-1
fs = PRF_per_va*va;
tpri = 1/fs;
D = 2*0.2704; %true physical centre separation

%input parameters
vy0 = -4;
vx0 = 3;
x0 = 0; %initial target x-position [m]
y0 = sqrt(R0^2 - h^2); %initial target y-position [m]
delta_t = 0; %tb error or offset expressed in [s]

%calculated parameters
tb = x0/(va-vx0);
yb = y0 + vy0*tb;
Rb = sqrt(yb^2 + h^2);
beta = 2*pi/lambda;
gamma = yb/Rb;
vrel =sqrt((vx0-va)^2 + (1-gamma^2)*vy0^2);

%Target signal length Ts:
Theta = 3; %3 degree for 3dB beamwidth
```

```
theta = Theta*pi/180; %convert to radians
az = int32(Rb*tan(theta/2)*5.14); %convert beam angle to sample number
az = double(az); %[samples]
Ts = 2*az*tpri; %[s] target signal length
T = 3.005*Ts; %total signal length
t1 = -(T-tpri)/2:tpri:(T-tpri)/2; %odd pulses
t2 = -(T-2*tpri)/2:tpri:T/2; %even pulses

%generate transmit signal range history
m = -15:2:15;
t1_mat = repmat(t1',[1 length(m)]);
m1_mat = repmat(m,[length(t1) 1]);
x1_mat = x0 + vx0*t1_mat;
y1_mat = y0 + vy0*t1_mat;
Rt1 = sqrt( (x1_mat - (va*t1_mat)).^2 + y1_mat.^2 + h^2 ); %transmit range history
Rr1 = sqrt( (x1_mat - (va*t1_mat - m1_mat*D/16)).^2 + y1_mat.^2 + h^2 ); %receive range history
s1 = rectpuls(t1_mat - (tb + delta_t),Ts).*exp(-j*beta*(Rt1 + Rr1));

t2_mat = repmat(t2',[1 length(m)]);
m2_mat = repmat(m,[length(t2) 1]);
x2_mat = x0 + vx0*t2_mat;
y2_mat = y0 + vy0*t2_mat;
Rt2 = sqrt( (x2_mat - (va*t2_mat)).^2 + y2_mat.^2 + h^2 ); %transmit range history
Rr2 = sqrt( (x2_mat - (va*t2_mat - m2_mat*D/16)).^2 + y2_mat.^2 + h^2 ); %receive range history
s2 = rectpuls(t2_mat - (tb + delta_t),Ts).*exp(-j*beta*(Rt2 + Rr2));

%sub-aperture assignment
m1 = 1:4;
m2 = 5:8;
m3 = 9:12;
m4 = 13:16;

%generate sub-apertures
ch1 = sum(s1(:,m1),2);
ch2 = sum(s2(:,m2),2);
ch3 = sum(s1(:,m3),2);
```

```
ch4 = sum(s2(:,m4),2);

%generate clutter signals
xn = (-T/2:50*tpri:T/2)*va;
n = length(xn)
s1_clut = 0;
s2_clut = 0;
for xc = xn
    tb_clut = xc/va;
    Rct1 = sqrt((xc - (va*t1_mat)).^2 + y0^2 + h^2);
    Rcr1 = sqrt((xc - (va*t1_mat - m1_mat*D/16)).^2 + y0^2 + h^2);
    s1_clut = s1_clut + rectpuls(t1_mat-(tb_clut+delta_t),Ts).*exp(-j*beta*(Rct1+Rcr1));
    n = n-1
    Rct2 = sqrt((xc - (va*t2_mat)).^2 + y0^2 + h^2);
    Rcr2 = sqrt((xc - (va*t2_mat - m2_mat*D/16)).^2 + y0^2 + h^2);
    s2_clut = s2_clut + rectpuls(t2_mat-(tb_clut+delta_t),Ts).*exp(-j*beta*(Rct2+Rcr2));
end

%generate sub-apertures for clutter signals
ch1_clut = rectpuls(t1'-(tb+delta_t),Ts).*sum(s1_clut(:,m1),2);
ch2_clut = rectpuls(t2'-(tb+delta_t),Ts).*sum(s2_clut(:,m2),2);
ch3_clut = rectpuls(t1'-(tb+delta_t),Ts).*sum(s1_clut(:,m3),2);
ch4_clut = rectpuls(t2'-(tb+delta_t),Ts).*sum(s2_clut(:,m4),2);

%add target and clutter signals
ch1 = ch1 + ch1_clut;
ch2 = ch2 + ch2_clut; ch2r = shiftM(ch2,-((4*D/16)/va)/tpri + 1/2);
ch3 = ch3 + ch3_clut; ch3r = shiftM(ch3,-((8*D/16)/va)/tpri);
ch4 = ch4 + ch4_clut; ch4r = shiftM(ch4,-((12*D/16)/va)/tpri + 1/2);

%calculate theoretical fractional angle
N = length(t1);
frac_a = (2/pi)*acot(beta*N*vrel^2/(pi*Rb*fs^2));

%calculate theoretical ATI phase
ve = vrel^2/va + (vx0-va);
```

```
atiPhase = (beta*(D/2)*gamma*vy0/va + beta*(D/2)*ve*delta_t/Rb)*180/pi %toggle mode baseline is D not D/2

%compute fractional Fourier transfors
Ch1 = fracF(ch1,frac_a); figure; plot(abs(Ch1))
Ch2r = fracF(ch2r,frac_a);
Ch3r = fracF(ch3r,frac_a);
Ch4r = fracF(ch4r,frac_a);

%time-frequency plot of signals
tfPlotSig(ch1,fs)
tfPlotSig(ch1-ch2r,fs)
tfPlotSig(ch3r-ch4r,fs)
tfPlotSig(ch1-ch3r,fs)
tfPlotSig(ch1-ch4r,fs)

%calculate interferograms
ati1 = Ch1.*conj(Ch2r);
ati2 = Ch2r.*conj(Ch3r);
ati3 = (Ch1-Ch2r).*conj(Ch2r-Ch3r);
ati4 = (Ch2r-Ch3r).*conj(Ch3r-Ch4r);
ati5 = ati3 + ati4;

figure; polar(angle(ati1),abs(ati1),'x');
[ATImag,J] = max(abs(ati1));
atiPhase_max = angle(ati1(J,1))*180/pi;
title(['Measured ATI Phase 1 & 2 = ', num2str(atiPhase_max)]);
xlabel(['Theoretical ATI Phase = ', num2str(atiPhase)]);
ylabel(['ATI Phase Error = ', num2str(abs(atiPhase-atiPhase_max))]);

figure; polar(angle(ati2),abs(ati2),'^');
[ATImag,J] = max(abs(ati2));
atiPhase_max = angle(ati2(J,1))*180/pi;
title(['Measured ATI Phase 2 & 3 = ', num2str(atiPhase_max)]);
xlabel(['Theoretical ATI Phase = ', num2str(atiPhase)]);
ylabel(['ATI Phase Error = ', num2str(abs(atiPhase-atiPhase_max))]);
```

```
figure; polar(angle(ati3),abs(ati3),'square');
[ATImag,J] = max(abs(ati3));
atiPhase_max = angle(ati3(J,1))*180/pi;
title(['Measured ATI Phase dpca1 & dpca2 = ', num2str(atiPhase_max)]);
xlabel(['Theoretical ATI Phase = ', num2str(atiPhase)]);
ylabel(['ATI Phase Error = ', num2str(abs(atiPhase-atiPhase_max))]);

figure; polar(angle(ati4),abs(ati4),'square');
[ATImag,J] = max(abs(ati4));
atiPhase_max = angle(ati4(J,1))*180/pi;
title(['Measured ATI Phase dpca2 & dpca3 = ', num2str(atiPhase_max)]);
xlabel(['Theoretical ATI Phase = ', num2str(atiPhase)]);
ylabel(['ATI Phase Error = ', num2str(abs(atiPhase-atiPhase_max))]);

figure; polar(angle(ati5),abs(ati5),'square');
[ATImag,J] = max(abs(ati5));
atiPhase_max = angle(ati5(J,1))*180/pi;
title(['Measured ATI Phase of ati1 + ati2 = ', num2str(atiPhase_max)]);
xlabel(['Theoretical ATI Phase = ', num2str(atiPhase)]);
ylabel(['ATI Phase Error = ', num2str(abs(atiPhase-atiPhase_max))]);
```

DOCUMENT CONTROL DATA

(Security classification of title, body of abstract and indexing annotation must be entered when document is classified)

1. ORIGINATOR (the name and address of the organization preparing the document. Organizations for whom the document was prepared, e.g. Centre sponsoring a contractor's report, or tasking agency, are entered in section 8.)

   Defence R&D Canada – Ottawa
   3701 Carling Avenue, Ottawa, Ontario, Canada K1A 0Z4

2. SECURITY CLASSIFICATION (overall security classification of the document including special warning terms if applicable).

   UNCLASSIFIED

3. TITLE (the complete document title as indicated on the title page. Its classification should be indicated by the appropriate abbreviation (S,C,R or U) in parentheses after the title).

   A Simulation Study of Multi-Channel RADARSAT-2 GMTI

4. AUTHORS (last name, first name, middle initial)

   Chiu, S.

5. DATE OF PUBLICATION (month and year of publication of document)	6a. NO. OF PAGES (total containing information. Include Annexes, Appendices, etc).	6b. NO. OF REFS (total cited in document)
November 2006	72	24

7. DESCRIPTIVE NOTES (the category of the document, e.g. technical report, technical note or memorandum. If appropriate, enter the type of report, e.g. interim, progress, summary, annual or final. Give the inclusive dates when a specific reporting period is covered).

   Technical Memorandum

8. SPONSORING ACTIVITY (the name of the department project office or laboratory sponsoring the research and development. Include address).

   Defence R&D Canada – Ottawa
   3701 Carling Avenue, Ottawa, Ontario, Canada K1A 0Z4

9a. PROJECT NO. (the applicable research and development project number under which the document was written. Specify whether project).	9b. GRANT OR CONTRACT NO. (if appropriate, the applicable number under which the document was written).
15eg	

10a. ORIGINATOR'S DOCUMENT NUMBER (the official document number by which the document is identified by the originating activity. This number must be unique.)	10b. OTHER DOCUMENT NOs. (Any other numbers which may be assigned this document either by the originator or by the sponsor.)
DRDC Ottawa TM 2006-209	

11. DOCUMENT AVAILABILITY (any limitations on further dissemination of the document, other than those imposed by security classification)

   (X) Unlimited distribution
   ( ) Defence departments and defence contractors; further distribution only as approved
   ( ) Defence departments and Canadian defence contractors; further distribution only as approved
   ( ) Government departments and agencies; further distribution only as approved
   ( ) Defence departments; further distribution only as approved
   ( ) Other (please specify):

12. DOCUMENT ANNOUNCEMENT (any limitation to the bibliographic announcement of this document. This will normally correspond to the Document Availability (11). However, where further distribution beyond the audience specified in (11) is possible, a wider announcement audience may be selected).

13. ABSTRACT (a brief and factual summary of the document. It may also appear elsewhere in the body of the document itself. It is highly desirable that the abstract of classified documents be unclassified. Each paragraph of the abstract shall begin with an indication of the security classification of the information in the paragraph (unless the document itself is unclassified) represented as (S), (C), (R), or (U). It is not necessary to include here abstracts in both official languages unless the text is bilingual).

Accurate ground moving target indication (GMTI) and target parameter estimation can be achieved only after sufficient suppression of interfering stationary clutter, particularly for space-based SARs with typically small exo-clutter regions. In its simplest form, this is accomplished using two radar receiver channels, such as the dual receive antenna mode of RADARSAT-2's Moving Object Detection EXperiment (MODEX). In this mode of operation, the full antenna is broken up into two sub-apertures with two parallel receivers to create two independent phase centres. It is well known, however, that a two-aperture approach to GMTI is sub-optimum and that target parameter estimation is often compromised by clutter interference or poor signal-to-clutter ratios. Two degrees-of-freedom are simply not enough to simultaneously suppress the clutter and to accurately estimate the target's properties, such as velocity and location.

The investigation, described in this Technical Memorandum, explores several concepts of increasing the spatial diversity for RADARSAT-2, which allows the two-channel SAR system to operate like a three or four channel radar. Owing to the very flexible programming capabilities of the RADARSAT-2 antenna, this can either be accomplished by the toggling of the transmitter between subsequent pulses or via clever transmitter/receiver excitation schemes. A trade-off analysis between number of channels, phase centre separations, and PRF limitations is presented for a system based on RADARSAT-2 MODEX parameters.

14. KEYWORDS, DESCRIPTORS or IDENTIFIERS (technically meaningful terms or short phrases that characterize a document and could be helpful in cataloguing the document. They should be selected so that no security classification is required. Identifiers, such as equipment model designation, trade name, military project code name, geographic location may also be included. If possible keywords should be selected from a published thesaurus. e.g. Thesaurus of Engineering and Scientific Terms (TEST) and that thesaurus-identified. If it not possible to select indexing terms which are Unclassified, the classification of each should be indicated as with the title).

multi-channel
multi-aperture
Ground Moving Target Indication (GMTI)
Parameter Estimations

Defence R&D Canada

Canada's leader in Defence
and National Security
Science and Technology

R & D pour la défense Canada

Chef de file au Canada en matière
de science et de technologie pour
la défense et la sécurité nationale

www.drdc-rddc.gc.ca